Energy and Mass-Number Dependence of Hadron-Nucleus Total Reaction Cross Sections

Akihisa Kohama,[1] Kei Iida,[1,2] and Kazuhiro Oyamatsu[1,3]

[1]*RIKEN Nishina Center, RIKEN, 2-1 Hirosawa, Wako-shi, Saitama 351-0198, Japan*
[2]*Department of Natural Science, Faculty of Science, Kochi University, Kochi 780-8520, Japan*
[3]*Department of Human Informatics, Aichi Shukutoku University, 2-9 Katahira, Nagakute, Aichi, 480-1197, Japan*

We thoroughly investigate how proton-nucleus total reaction cross sections depend on the target mass number A and the proton incident energy. In doing so, we systematically analyze nuclear reaction data that are sensitive to nuclear size, namely, proton-nucleus total reaction cross sections and differential elastic cross sections, using a phenomenological black-sphere approximation of nuclei that we are developing. In this framework, the radius of the black sphere is found to be a useful length scale that simultaneously accounts for the observed proton-nucleus total reaction cross section and first diffraction peak in the proton elastic differential cross section. This framework, which is shown here to be applicable to antiprotons, is expected to be applicable to any kind of projectile that is strongly attenuated in the nucleus. On the basis of a cross-section formula constructed within this framework, we find that a less familiar $A^{1/6}$ dependence plays a crucial role in describing the energy dependence of proton-nucleus total reaction cross sections.

1. Introduction

The total reaction cross section (σ_R) of nuclei is one of the most fundamental observables in nuclear physics, which helps us to know nuclear radii and even nuclear density distributions. The role of σ_R in deducing the nuclear density distributions is complementary to that of the differential cross section of elastic scattering, and both of them are governed by diffraction phenomena.[1)] On the other hand, nuclear masses and radii characterize the bulk properties of nuclei. In fact, the saturation of the binding energy and density deduced from systematic data for the masses and charge radii of stable nuclei reflects the behavior of the equation of state of nearly symmetric nuclear matter near the saturation density.[2,3)]

As is well known, the nuclear radii and density distributions are deduced from electron and proton elastic scattering off nuclei .[4–7)] To deduce the matter density distributions and radii, during the past four decades there have been many efforts of studying proton elastic scattering cross sections, which are based on various scattering theories incorporating empirical nucleon-nucleon scattering amplitudes, such as the Glauber approximation[4,6)] and nonrelativistic and relativistic optical potential methods .[8–12)]

We here choose a different approach: We start from a naive but firm framework, namely, the Fraunhofer diffraction, which is expected to set qualitative standards for nuclear size. Unexpectedly, this framework turns out to be quantitatively very sound, which will be explained below.

For the purpose of deducing nuclear size from proton-nucleus elastic scattering and σ_R, we proposed a model in which a nucleus is viewed as a "black" (i.e., strongly absorptive to incident protons) sphere of radius "a", which is called a black-sphere (BS) approximation of nuclei.[1,13,14)] This BS radius, a, plays a central role in this framework. We determine a by fitting the angle of the first elastic diffraction peak calculated for proton diffraction by a circular black disk of radius a to the measured value. For incident protons of energy above 800 MeV, it was found that πa^2 agrees with the measured σ_R within error bars. It can thus be regarded as a "reaction radius" inside which the reaction with incident protons occurs.

Within the BS framework, we developed a formula for σ_R of proton-nucleus reactions as a function of the mass number (A) and the neutron excess of the target nucleus and proton incident energy T_p in a way free from any adjustable T_p-dependent parameter.[15)] We deduce the dependence of σ_R on T_p from a simple argument involving the nuclear "optical" depth for absorption of projectiles. We call the formula the BS cross-section formula .[16)] The only scale included in the formula is set by the BS radius a, which is determined in the same way as described above.[14)] For stable nuclei, this formula reproduces the empirical T_p dependence of σ_R at T_p = 100–1000 MeV remarkably well. In this formula, the T_p dependence of a is determined by that of proton-nucleon total cross sections, while the target mass-number dependence of a is sensitive to the surface thickness of the target nucleus. This formula can be easily extended to nucleus-nucleus reactions and is shown to well reproduce the empirical data for energies above 100 MeV/nucleon.[15,17)]

Due to its suitability for systematic calculations, the present formula is incorporated into the Particle and Heavy Ion Transport code System (PHITS).[18–20)] In the code, the formula is used for systematic evaluations of σ_R, which in turn determine how often the incident particles collide with nuclei in a material. The application area of this code is very broad, which ranges from the fields of accelerator technology, particle therapy, and space radiation to many other fields that are related to particle and heavy-ion transport phenomena.

In this paper, we revisit a complicated A and T_p dependence of the proton-nucleus total reaction cross sections. In doing so, we will put emphasis on the fact that the BS radius is the length scale that simultaneously accounts for the observed σ_R of proton-nucleus reaction and diffraction peak in the proton elastic differential cross section. After summarizing the successive works on our systematic analyses based on the BS approximation of nuclei, we examine the T_p and A dependence of σ_R carefully. A part of the results have been already reported in refs.[13–15,17)]

This paper is organized as follows: In Sec. 2, we overview our BS approximation of nuclei. In Sec. 3, we summarize how data look like from the viewpoint of the BS approximation. In Sec. 4, we briefly review the BS cross-section formula, which was developed in ref.,[15] and analytically examine its A dependence. Detailed derivation of the formula can be found in Sec. 3 of ref.[21] We extend this framework to such probes as antiprotons in Sec. 5. Finally we give a summary in Sec. 6.

In collecting the empirical data, we have made access to Experimental Nuclear Reaction Data File (EXFOR).[22] As for the criterion to adopt the data for σ_R, we have accepted the data which are to within 15 % from the systematic behavior of various data sets. We use units in which $\hbar = c = 1$.

2. Black-Sphere (BS) Approximation

In this section, we introduce the BS approximation of nuclei,[13,14] which can be regarded as a "contemporary" BS model as compared with the original one[1] (hereafter referred to as "classical"). We regard the former as contemporary, because it is based on the quantitative reproducibility of available σ_R data, while the classical one aims at qualitatively describing a global behavior of the elastic diffraction patterns. The formal definition of the contemporary BS approximation will be given below via Eq. (2.7).

For convenience, we restrict ourselves to the case of proton projectiles, but the concept can be easily extended to such hadronic probes as neutrons, antiprotons, pions, and kaons. The case of antiprotons will be described in Sec. 5. Possible extension of this framework to proton inelastic scattering has been discussed recently,[23] but will not be discussed here.

We here emphasize that our contemporary BS model is *not* the eikonal approximation with the rectangular density distribution although the connection with it can be clearly shown as in Sec. 2 of ref.[21] Since, for stable nuclei, the accuracy of $\sigma_R \simeq \sigma_{\rm BS}$ of proton-nucleus ($A \geq 3$) and nucleus-nucleus reactions ($A_P, A_T \lesssim 50$), where $A_{P(T)}$ is the mass number of a projectile (target), has been confirmed within a few %,[14,15] the indication by Alkhazov *et al*.[24,25] that the results of our BS model are not accurate enough particularly for light nuclei is not appropriate in the context of σ_R.

Blair *et al*. developed the celebrated "sharp cutoff" model for low energy alpha-particle elastic scattering off nuclei several decades ago,[26,27] which is a strong absorption model that can be obtained from wave optics by cutting off the interaction range or the partial-wave (impact parameter) window. This model reproduces a global behavior of the alpha-nucleus scattering fairly well.[26,27] In fact, the BS approximation is similar in concept and structure to the "sharp cutoff" model, but how to relate between them is not obvious partly because the geometrical size of alpha particles is treated differently and partly because the definition of the "sharp cutoff" radius is based on the behavior of partial waves rather than the nuclear density distribution.

2.1 Applicability

We begin by regarding a target nucleus for proton elastic scattering as a black sphere of radius a. This picture holds when the target nucleus is strongly absorptive to the incident proton and hence acts like a black sphere. It is important to notice that the interaction between the incident proton and the target nucleus is strong but not infinitely strong; otherwise the incident proton could be sensitive to an exponentially low density region, and hence any place would be black.

For incident kinetic energy T_p above $\sim$ 800 MeV, the optical potential for this reaction is in fact strongly absorptive. It can be essentially viewed as a superposition of the nucleon-nucleon scattering amplitudes. Since the imaginary part of the amplitude is dominant over the real part in this energy range, the BS picture is applicable to a first approximation.

Another requirement for the BS picture is that the proton wave length is considerably shorter than the nuclear size. For proton incident energies higher than about 800 MeV, both requirements are basically satisfied. This approximation was originally used by Placzek and Bethe[1] in describing the elastic scattering of fast neutrons.

Since one can regard the proton beam as a plane wave of momentum $p_{\rm Lab}$ in the laboratory frame,

$$p_{\rm Lab} = \sqrt{(T_p + m_p)^2 - m_p^2} \tag{2.1}$$

with the proton mass, m_p, the BS approximation can be described in terms of wave optics. This picture reduces to a diffraction of the wave by a circular black disk of radius a if the corresponding wave optics is close to the limit of geometrical optics, i.e.,

$$\frac{a}{\lambda_{\rm Lab}} \gg 1, \tag{2.2}$$

where $\lambda_{\rm Lab} = 2\pi/p_{\rm Lab}$ is the wave length. We will consider in the next section the range of T_p in which $a/\lambda_{\rm Lab} \gg 1$ is satisfied. According to Babinet's principle, this diffraction is in turn equivalent to the Fraunhofer diffraction by a hole of the same shape as the disk embedded in a screen.[28]

The scattering amplitude for this diffraction in the center-of-mass (c.m.) frame of the proton and the nucleus reads

$$f(\mathbf{q}) = ipaJ_1(qa)/q, \tag{2.3}$$

where $\mathbf{q}$ is the momentum transfer, $\mathbf{p}$ is the proton momentum in the c.m. frame, and $J_n(x)$ is the n-th order Bessel function. With this amplitude, we obtain the differential cross section of proton-nucleus elastic scattering as

$$\frac{d\sigma}{d\Omega} = |f(\mathbf{q})|^2. \tag{2.4}$$

The relation of the BS approximation to the conventional scattering theory can be found in Sec. 2 of ref.[21]

We note that the BS picture is fairly successful in describing the elastic scattering of low energy α particles.[7,26,27] It was also used for analyses of the scattering of intermediate-energy pions and low-energy antiprotons.[7]

2.2 How to Determine "a"

The scale "a" is the only undetermined parameter in the scattering amplitude of Eq. (2.3). We determine it using the empirical differential cross sections of proton-nucleus elastic scattering.

The c.m. scattering angle for proton elastic scattering is generally given by

$$\theta_{\rm c.m.} = 2\sin^{-1}(q/2p). \tag{2.5}$$

For the proton diffraction by a circular black disk of radius a, we can calculate the value of $\theta_{\rm c.m.}$ at the first peak as a function of a. (Here we define the zeroth peak as that whose

angle corresponds to $\theta_{\rm c.m.} = 0$.) We determine a in such a way that this value of $\theta_{\rm c.m.}$ agrees with the first peak angle for the measured diffraction in proton-nucleus elastic scattering, θ_M. The radius, a, and the angle, θ_M, are then related by

$$2pa\sin(\theta_M/2) = 5.1356\cdots . \tag{2.6}$$

This is obtained by requiring that the derivative of the cross section with respect to the scattering angle be zero. To be explicit, we write

$$a = \frac{5.1356\cdots}{2p\sin(\theta_M/2)}. \tag{2.7}$$

We call this the BS radius formula. As was discussed analytically in the eikonal approximation,[29] the oscillation period in the diffraction pattern is determined by the nuclear radius, which is closely related with the concept underlying Eq. (2.7).

The determination of a from the first peak angle, rather than the first dip angle, is the key to the success of the present quantitatively sound approach.

2.3 *Definition of $\sigma_{\rm BS}$ and $r_{\rm BS}$*

Within the present BS approximation, we calculate the proton-nucleus total reaction cross section, σ_R, from a. This approximation regards it as the geometrical cross section,

$$\sigma_{\rm BS} \equiv \pi a^2. \tag{2.8}$$

Here we assume that the incident protons are point particles, leading to vanishing contribution from the proton size to $\sigma_{\rm BS}$.[14] This is reasonable because the measured proton-proton reaction cross section ($\sigma_{pp}^{\rm reaction} \equiv \sigma_{pp}^{\rm total} - \sigma_{pp}^{\rm elastic}$) is relatively small at T_p less than $\sim$ 1000 MeV, where $\sigma_{pp}^{\rm total}$ ($\sigma_{pp}^{\rm elastic}$) is the proton-proton total (elastic) cross section. Once one accepts the scattering amplitude of the Fraunhofer scattering for describing the reactions,[13] one naturally obtains expression (2.8) (see Sec. 2 of ref.[21]). By substituting the values of a determined by Eq. (2.7) into Eq. (2.8), we evaluate $\sigma_{\rm BS}$ for various nuclei at various proton energies.

The BS approximation is also applicable for analyzing nuclear matter radii. For simplicity, we assume that the density distribution of the black sphere is uniform, i.e., a rectangular nucleon distribution. Then we can naturally write the root-mean-square (rms) BS radius, $r_{\rm BS}$, as

$$r_{\rm BS} \equiv \sqrt{3/5}a. \tag{2.9}$$

The factor $\sqrt{3/5}$ comes from the second moment of the rectangular density distribution. The values of $r_{\rm BS}$ are to be compared with the empirically deduced values of the rms matter radius, r_m, and in fact will turn out to be in good agreement with r_m at $T_p \gtrsim 800$ MeV and $A \gtrsim 50$.

3. How Do the Data Look Like?

In this section, we overview proton scattering data and analyze them within the framework of the BS approximation.

3.1 *Resolution*

For validity of the BS approximation, the scattering should be close to the limit of the geometrical optics, as mentioned in the previous section. This condition is fairly well satisfied at least for $T_p \gtrsim 800$ MeV, since $a/\lambda_{\rm Lab}$ is well above unity even for ^{4}He. The existence of the first diffraction peak is a good measure to check the validity of the present approximation as a function of energy. In fact, it is indispensable in our formulation to determine the value of a from the empirical diffraction peak angle of proton-nucleus elastic scattering.

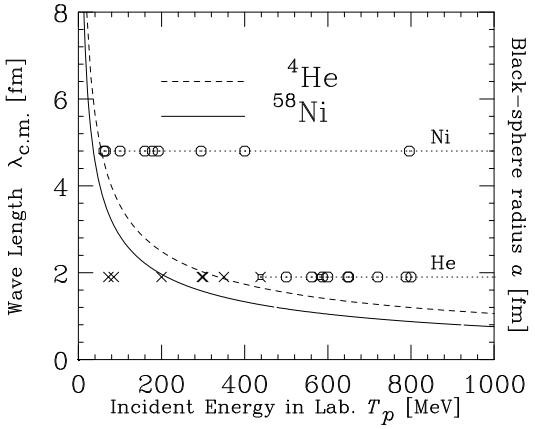

Fig. 1. Comparison of the BS radius, a, at $T_p \simeq 800$ MeV with the c.m. de Broglie wave length of an incident proton of kinetic energy T_p in the laboratory frame for the target of ^{4}He (^{58}Ni). We draw the dashed (solid) curve for the de Broglie wave length for ^{4}He (^{58}Ni). The dotted lines show the BS radius a of ^{4}He and ^{58}Ni at about 800 MeV. On top of those lines, we plot the circles (crosses) in the case in which the first peak of the diffraction appears (disappears). The square with cross at 438 MeV for ^{4}He implies that the first peak is not clear due to the quality of the data.

In order to examine the correspondence between the peak existence and the ratio of the BS radius a at $T_p \gtrsim 800$ MeV to the proton de Broglie wave length, $\lambda_{\rm c.m.} = 2\pi/p$, in the c.m. frame, we plot in Fig. 1 the "won-and-lost records" which distinguish between the presence and absence of the diffraction peak. Note that the T_p dependence of the BS radius is much weaker than that of $\lambda_{\rm c.m.}$ as we shall see.

For ^{4}He, we adopt the data of $T_p = 72$ MeV,[30] $T_p = 85$ MeV,[31] $T_p = 200, 350, 500$ MeV,[32] $T_p = 297$ MeV,[33] $T_p = 300$ MeV,[34] $T_p = 438, 648, 1036$ MeV,[35] $T_p = 350, 650, 1050, 1150$ MeV,[36] $T_p = 561, 800, 1029$ MeV,[37] $T_p = 580, 720$ MeV,[38] $T_p = 587$ MeV,[39] $T_p = 600$ MeV,[40] and $T_p = 788$ MeV.[41] For $T_p \gtrsim 800$ MeV, the references are listed in ref.[14]

For ^{58}Ni, we adopt the data of $T_p = 61.4$ MeV,[42] $T_p = 65$ MeV,[43,44] $T_p = 100.4$ MeV,[45] $T_p = 160$ MeV,[46] $T_p = 178$ MeV,[47] and $T_p = 192, 295, 400$ MeV.[11] For $T_p \gtrsim 800$ MeV, the references are listed in ref.[13]

As the incident energy decreases, the oscillation becomes broader and more blurred, and eventually the first peak disappears around $\lambda_{\rm c.m.}/a \simeq 1$, as shown in Fig. 1. It is clearly shown in Fig. 2(a) of ref.[44] how the measured diffraction peaks disappear at $T_p = 65$ MeV for ^{16}O–^{40}Ca. At this energy, the de Broglie wave length is around 4 fm, which is of order the values of a at 800 MeV for such targets as ^{20}Ne and ^{24}Mg. Thus, the presence of the diffraction peaks is closely related to the nuclear size. As will be mentioned in the next subsection, the value of a at $T_p \simeq 800$ MeV, multiplied by $\sqrt{3/5}$, is surprisingly close to r_m for $A \gtrsim 50$.

3.2 $T_p \gtrsim 800$ *MeV*

In refs.,[13,14] we clarified two salient features from the data of incident energies higher than $\sim$ 800 MeV. First, the absorption cross section $\sigma_{\rm BS}$, Eq. (2.8), agrees with the empirical

total reaction cross section within error bars, i.e.,

$$\sigma_R \simeq \sigma_{\rm BS}, \tag{3.1}$$

although the comparison is possible only for stable nuclei such as C, Sn, and Pb.[14] We will show later that this feature is persistent down to $T_p \sim 100$ MeV. We thus see the role played by $\sigma_{\rm BS}$ in predicting σ_R. This is useful for nuclides for which elastic scattering data are available but no data for σ_R are available. Second, $r_{\rm BS}$, Eq. (2.9), almost completely agrees with the empirically deduced values of r_m for $A \gtrsim 50$, while it systematically deviates from the deduced values for $A \lesssim 50$.

Let us examine the case of $A \lesssim 50$ in more details. For light nuclei, the oscillation period in the elastic diffraction becomes broader as A decreases.[29] Equation (2.7) implies that when a becomes smaller, the value of θ_M becomes larger for fixed T_p. Since the value of θ_M itself is relatively large, the values of $\sigma_{\rm BS}$ and $r_{\rm BS}$ can be well determined despite the uncertainty in θ_M as compared to heavy nuclei. Therefore, better determination of $\sigma_{\rm BS}$ and $r_{\rm BS}$ would be possible for light nuclei than for heavy nuclei.

In contrast to the good agreement between $r_{\rm BS}$ and r_m for $A \gtrsim 50$, however, the values of $r_{\rm BS}$ are found to be systematically smaller than those of r_m for $A \lesssim 50$. A possible reason for this discrepancy is the change in the ratio between the surface and the bulk portions toward lighter nuclei. This change may induce a difference in the expansion series with respect to $A^{1/3}$ between $r_{\rm BS}$ and r_m, as discussed in Sec. 1.2 of Ref .[21] We remark that the induced difference is appreciable even for $A \gtrsim 50$, while the good agreement between $r_{\rm BS}$ and r_m suggests a counteracting effect due to developing neutron-skin thickness on the beta stability line[48] (see also Sec. 4 of ref. [21]).

From the observation of the global A dependence of the BS radius, a, we found that, for stable nuclei, the BS radius a scales as[14]

$$a \simeq 1.2135A^{1/3} \text{ fm}, \tag{3.2}$$

which will be hereafter referred to as the black-sphere scaling (BS scaling). Equivalently, from Eq. (2.9), we obtain[14]

$$r_{\rm BS} \simeq 0.9400A^{1/3} \text{ fm}, \tag{3.3}$$

and, from Eq. (2.8),

$$\sigma_{\rm BS} \simeq 46.263A^{2/3} \text{ mb}. \tag{3.4}$$

As one can see from Fig. 2, the agreement of the BS scaling with both the empirical values of $\sqrt{\sigma_R/\pi}$ and $\sqrt{\sigma_{\rm BS}/\pi}$ is fairly good.

For systematic evaluations of σ_R that can be applied for practical use, we have to aim at a better agreement with the empirical values beyond expression (3.4). For this purpose, we propose a couple of other parametrizations à la Carlson, which fit $(\sigma_R/\pi)^{1/2}$ in terms of a linear function in $A^{1/3}$:[49] The first one, denoted by BS-fit1, is given by

$$a = 1.2671A^{1/3} - 0.152 \text{ fm}. \tag{3.5}$$

We obtain this by χ^2-fitting of the linear function in $A^{1/3}$ to the values of $(\sigma_{\rm BS}/\pi)^{1/2}$. The standard deviation is around 0.096 fm. Note that this expression inevitably puts its emphasis on the region of $A < 50$, because most of the data points distribute in this region. By putting slightly more emphasis on the data points in the region of $A > 50$, we obtain the second one, BS-fit2, which is given by

$$a = 1.33A^{1/3} - 0.35 \text{ fm}. \tag{3.6}$$

Note that in Fig. 2 the BS-fit1 intervenes between the BS scaling and the BS-fit2, which differ only by of order 0.1 fm.

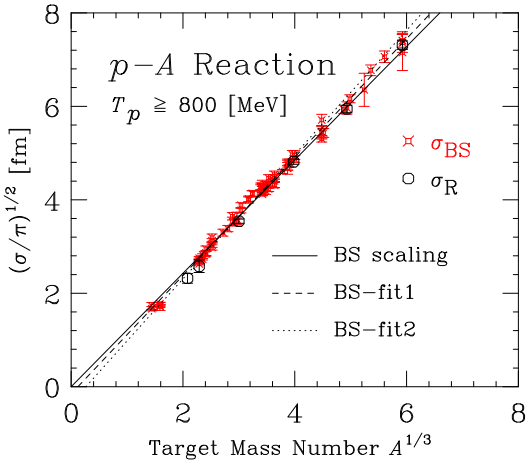

Fig. 2. (Color online) Comparison of the three fitting lines with the effective radius $\sqrt{\sigma_{\rm BS}/\pi}$ (crosses) for the absorption cross section of protons of $T_p \gtrsim 800$ MeV by a target nucleus of mass number A. The solid line denotes the BS scaling, Eq. (3.2), the dashed line the BS-fit1, Eq. (3.5), and the dotted line the BS-fit2, Eq. (3.6). We also plot the effective radius $\sqrt{\sigma_R/\pi}$ (dots) for the empirical data for ^{9}Be, ^{27}Al, C, Cu, Sn, and Pb. For the latter four elements the value of σ_R is the average over the natural isotopic abundance in a target. For these data, we set A as the mass number of the most abundant isotope and assign the uncertainty in A due to the natural abundance, as in Fig. 3 of ref.[14]

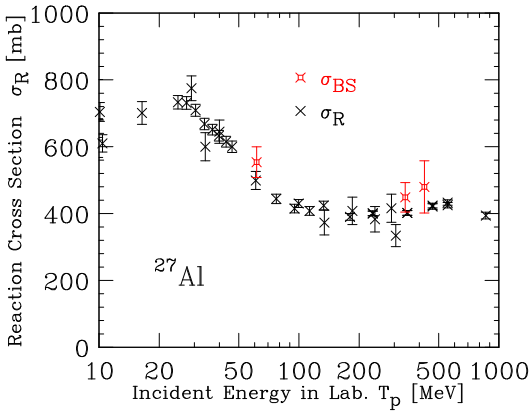

Fig. 3. (Color online) Energy dependence of $\sigma_{\rm BS}$ (squares with cross) for the reaction of protons on ^{27}Al. The values of $\sigma_{\rm BS}$ are obtained from the measured peak angle of the first diffraction maximum of the proton elastic scattering. The empirical data for σ_R (×) are taken from in ref.[49]

3.3 *Down to $T_p \simeq 50$ MeV*

Let us consider how the data look like when we decrease T_p from 800 MeV. As we have mentioned in Sec. 3.1 for a target of fixed A, the diffraction patterns become blurred as T_p decreases. At a certain value of T_p, the first diffraction peak tends to disappear. We find, however, that, as long as the peak exists, the relation (3.1) holds within the empirical uncertainties.

As an example, in Fig. 3, we plot the values of $\sigma_{\rm BS}$ for proton-^{27}Al reactions as a function of T_p. To obtain the val-

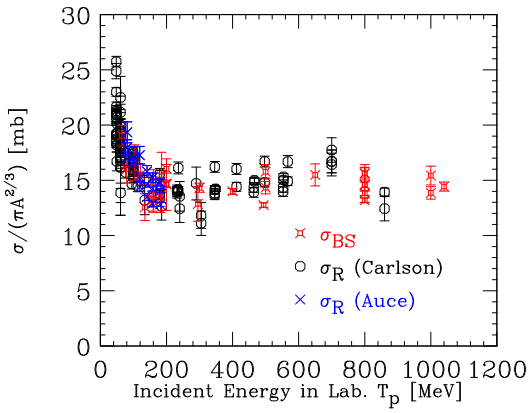

Fig. 4. (Color online) Comparison of the effective cross sectio $\sigma_{\rm BS}/(\pi A^{2/3})$ with $\sigma_R/(\pi A^{2/3})$ as a function of the kinetic energy of an in cident proton. The empirical data for σ_R are taken from the compilation b Carlson (○)[49] and the measurements by Auce *et al.* (×).[52] The values o $\sigma_{\rm BS}$ ($\equiv \pi a^2$), which are represented by squares with crosses, are obtaine from the measured peak angle of the first diffraction maximum of the proton elastic scattering. They are consistent with the measured σ_R.

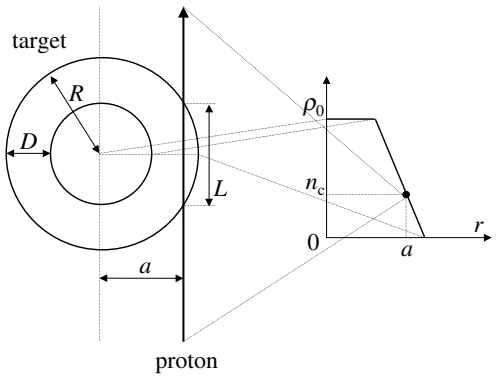

Fig. 5. Model for the density distribution of a target nucleus and the critical proton trajectory inside which the reaction with the target nucleus occurs. This is the same as Fig. 1 in ref.[15]

ues of a, we adopt the first peak angle of the empirical data for the differential cross sections of proton-^{27}Al elastic scattering at $T_p = 61.4$ MeV,[42] 340 MeV,[50] and 424 MeV.[51] Other examples will be shown later. From Fig. 3, we find that σ_R agrees with $\sigma_{\rm BS}$ within error bars, which ensures Eq. (3.1). This relation suggests that the radius a can be regarded as a "reaction radius," inside which the reaction with incident protons occurs. The above tendency holds for other stable nuclei, as shown in Fig. 4.

Note that the condition for Eq. (3.1) to hold is slightly different for the case of nucleus-nucleus reactions. As we have already shown in refs.,[15,17] the BS approximation can be extended to nucleus-nucleus reactions by using $\pi(a_P + a_T)^2$, where a_P (a_T) is the BS radius of a projectile (target). Interestingly, the empirical values of the total reaction cross section $\sigma_R(A + A)$ agree well with $\pi(a_P + a_T)^2$ for incident energies per nucleon down to 100 MeV, not only in the presence of the first diffraction peaks of proton elastic scattering that lead to a_P and a_T, but also in their absence in which case a_P and a_T are evaluated from Eq. (3.1) as $(\sigma_R/\pi)^{1/2}$.

4. Black-sphere (BS) Cross-Section Formula

In this section, we briefly review the BS cross-section formula, which was originally developed in ref.[15] for describing the proton-nucleus total reaction cross section σ_R, and analytically analyze the A dependence of the formula. The detailed derivation of the formula can be found in Sec. 3 of ref.[21]

The BS cross-section formula is constructed as a function of the mass and neutron excess of the target nucleus and T_p in a way free from any adjustable T_p-dependent parameter. The geometry of the reaction is assumed as can be seen in Fig. 5. We deduce the dependence of σ_R on T_p from a simple argument involving the nuclear "optical" depth for absorption of incident protons within the framework of the BS approximation of nuclei. This formula can be easily extended to nucleus-nucleus reactions.[15,17]

4.1 *Energy Dependence*

In setting the T_p dependence of the formula, we retain the expression for $\sigma_{\rm BS}$ given by Eq. (2.8), leading to

$$\begin{aligned}\tilde{\sigma}_{\rm BS}(T_p) &= \pi a(T_p)^2 \\ &= \pi a_0^2\left(1+\frac{\Delta a}{a_0}\right)^2, \end{aligned} \tag{4.1}$$

where $\Delta a \equiv a(T_p) - a_0$, and a_0 denotes the value of a determined at 800 MeV for each nucleus. While Eqs. (3.2), (3.5), and (3.6) introduced in Sec. 3.2 are helpful for estimating a_0, Δa is responsible for the energy dependence of $\sigma_{\rm BS}$. We introduce the *effective* nuclear optical depth τ defined by

$$\tau = \bar{\sigma}_{pN}^{\rm total} n_c L', \tag{4.2}$$

with

$$\bar{\sigma}_{pN}^{\rm total} = (Z/A)\sigma_{pp}^{\rm total} + (1 - Z/A)\sigma_{pn}^{\rm total}, \tag{4.3}$$

where $\sigma_{pp(pn)}^{\rm total}$ is the proton-proton (neutron) total cross section, n_c is the critical nucleon density at the distance of $r = a$ from the nuclear center, and L' is the length of the part of the critical trajectory in which the total nucleon density is lower than n_c while being above zero (see Fig. 5).

By assuming that $\tau = 0.9$ independently of T_p, we express the T_p dependence of $\Delta a/a_0$ as that driven solely by $\bar{\sigma}_{pN}^{\rm total}$. The T_p-*in*dependent part of $\Delta a/a_0$ is described by several parameters that characterize the density distribution of the target nucleus assumed to be trapezoidal, which makes the expression for Δa analytically tractable. The choice of the value of 0.9 for τ is reasonable since this is consistent with the values of a_0 and n_c for ^{12}C, ^{58}Ni, ^{124}Sn, and ^{208}Pb listed in Table 1 of ref.[21] The detailed description of the formula is given in the original paper[15] and in Sec. 3 of ref.[21] in which minor corrections to the T_p-independent part of $\Delta a/a_0$ described in ref.[15] will be added.

The comparison with the empirical data is shown in Fig. 6. We find that, for stable nuclei, this formula remarkably well reproduces the empirical T_p dependence of σ_R at $T_p = 100$–1000 MeV, where the deviation of $\bar{\sigma}_{pN}^{\rm total}$ from its empirical

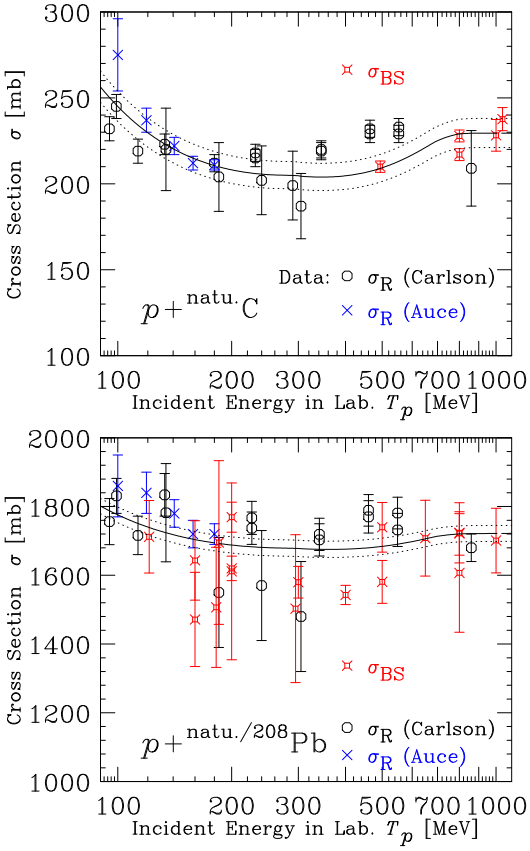

Fig. 6. (Color online) Comparison of the BS cross-section formula (solid curve) with the empirical values for $\sigma_R(p + {}^{\text{natu.}}\text{C})$ (upper) and $\sigma_R(p + {}^{\text{natu./}208}\text{Pb})$ (lower) as a function of the kinetic energy of an incident proton. We adopt the BS radius, a_0, at 800 MeV as 2.70 ± 0.05 fm for carbon and 7.40 ± 0.05 fm for lead. The uncertainties, whose assignment is the same as in ref.,[13] are shown by the dotted curves. We also plot the empirical data for σ_R from the compilation by Carlson (○)[49] and the measurements by Auce *et al.* (×).[52] Note that the data of 220 MeV $\leq T_p \leq$ 570 MeV[53] turn out to be systematically large. The values of σ_{BS} ($\equiv \pi a^2$), which are represented by squares with crosses, are obtained from the measured peak angle of the first diffraction maximum of the proton elastic scattering. They are consistent with the measured σ_R.

value at $T_p = 800$ MeV is small enough to validate the present formulation. We remark in passing that the contribution from the Coulomb interaction, which is not included in this framework, can be safely neglected in this energy region.[15]

We also plot the values of σ_{BS} in the figure. For obtaining these values, we adopt the empirical data for the differential cross sections of proton-C elastic scattering at $T_p = 494.0$ MeV in ref.[54] For $T_p \gtrsim 800$ MeV, the references of the data are listed in ref.[14] For elastic scattering data of ^{208}Pb, we adopt the empirical values at $T_p = 65$ MeV,[44] $T_p = 80, 121, 160, 182$ MeV,[55] $T_p = 160$ MeV,[46] $T_p = 185$ MeV,[56] $T_p = 200$ MeV,[57,58] $T_p = 200, 300, 400, 500$ MeV,[59] $T_p = 295$ MeV,[12] $T_p = 500$ MeV,[60] and $T_p = 650$ MeV.[61] We do not adopt the data at $T_p = 100.4$ MeV,[45] because the measured diffraction pattern does not include the first peak. For $T_p \gtrsim 800$ MeV, the references are listed for p+^{208}Pb in ref.[13]

For comparison, we plot the present BS cross-section formula together with other empirical formulas in Fig. 7. We choose those constructed only for nucleon-nucleus reactions, which are summarized in Sec. 6 of ref.[21] The present formula alone reproduces the T_p dependence in a manner that is

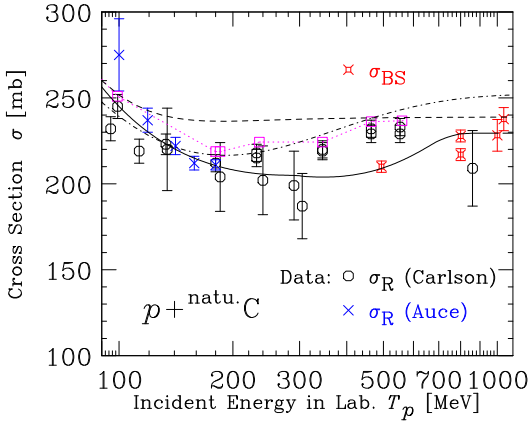

Fig. 7. (Color online) Comparison of various empirical formulas for $\sigma_R(p + \text{C})$ with the empirical values as a function of T_p. The values of Carlson's formula obtained by using the parameters listed in Table A of ref.[49] are plotted by the squares with dotted line. The values of the same formula but using the parametrization of Machner *et al.*[62] are drawn by the dashed curve. The values of Letaw's formula[63] are drawn by the dot-dashed curve. The values of the BS cross-section formula with $a_0 = 2.70$ fm are drawn by the solid curve. The empirical values and the values of σ_{BS} are the same as in Fig. 6.

consistent with the latest empirical data,[52] which are systematically more reliable.

4.2 *Mass-Number (A) Dependence*

This section provides a main part of the present paper. Here, we examine the A dependence of the BS cross-section formula,

$$\tilde{\sigma}_{\text{BS}}(T_p) = \pi a_0^2 \left[1 + \left(\frac{\rho_0 a_0}{D n_{c0}} - \frac{a_0}{L'_0} \left. \frac{dL'}{da} \right|_0 \right)^{-1} \frac{\Delta\bar{\sigma}^{\text{total}}_{pN}}{\bar{\sigma}^{\text{total}}_{pN0}} \right]^2 . \tag{4.4}$$

The definition of each term in this formula can be found in Sec. 3 of ref.,[21] together with the derivation of Eq. (4.4) (or, equivalently, Eq. (3.12) of ref.[21]).

First, we examine the A dependence of the key terms in the above expression. Hereafter, just like a_0, we will affix "0" to the T_p dependent quantities whenever we mean the values at $T_p = 800$ MeV. Following the definition of L', Eq. (3.4) of ref.,[21] the A dependence of the path length, L', can be expressed as

$$\begin{aligned} L' &= 2\sqrt{R^2 - a^2} \\ &= 2\sqrt{(R+a)(R-a)} \\ &\propto A^{1/6} D^{1/2}, \end{aligned} \tag{4.5}$$

where $D(= 2.2\text{fm})$ is a constant as given in Eq. (3.10) of ref.[21]

Another key term is $\rho_0 a_0/(D n_{c0})$ in the coefficient of $\bar{\sigma}_{pN}$ found in expression (4.4). Since $a_0 \propto A^{1/3}$ and $n_{c0} \propto L'^{-1} \propto A^{-1/6} D^{-1/2}$, we may write

$$\frac{\rho_0 a_0}{D n_{c0}} \propto D^{-1/2} A^{1/2}, \tag{4.6}$$

where $\rho_0 = 0.16$ fm^{-3}.

We next examine the coefficient of $\Delta\bar{\sigma}^{\text{total}}_{pN}/\bar{\sigma}^{\text{total}}_{pN0}$, i.e.,

$$\left(\frac{\rho_0 a_0}{D n_{c0}} - \frac{a_0}{L'_0} \left. \frac{dL'}{da} \right|_0 \right)^{-1}, \tag{4.7}$$

in Eq. (4.4). To examine the A dependence of the second term in the parenthesis of Eq. (4.7), we look into the term $dL'/da|_0$ (see Eq. (3.19) of ref.[21]). We obtain

$$\frac{\rho_0 a_0}{Dn_{c0}} - \frac{a_0}{L'_0}\left.\frac{dL'}{da}\right|_0 = \frac{\rho_0 a_0}{Dn_{c0}}\left\{1 + 4\frac{Dn_{c0}}{\rho_0 a_0}\left(\frac{a_0}{L'_0}\right)^2\right\}. \quad (4.8)$$

Since the first term in the left side is much larger than the second term, we expand it as follows:

$$\left(\frac{\rho_0 a_0}{Dn_{c0}} - \frac{a_0}{L'_0}\left.\frac{dL'}{da}\right|_0\right)^{-1} = \frac{Dn_{c0}}{\rho_0 a_0} - 4\left(\frac{Dn_{c0}}{\rho_0 a_0}\right)^2\left(\frac{a_0}{L'_0}\right)^2 + \cdots. \quad (4.9)$$

This expansion becomes better as A increases. Thus, the first term gives the leading correction to πa_0^2 in the BS cross-section formula.

Finally, we obtain the following expression:

$$\tilde{\sigma}_{\rm BS}(T_p) \simeq \pi a_0^2 + 2\pi\left[\frac{Dn_{c0}}{\rho_0 a_0}a_0^2 + O\left(\left(\frac{Dn_{c0}a_0}{\rho_0 L'_0}\right)^2\right)\right]\frac{\Delta\bar{\sigma}_{pN}^{\rm total}}{\bar{\sigma}_{pN0}^{\rm total}} + O\left(\left(\frac{Dn_{c0}}{\rho_0}\right)^2\left(\frac{\Delta\bar{\sigma}_{pN}^{\rm total}}{\bar{\sigma}_{pN0}^{\rm total}}\right)^2\right). \quad (4.10)$$

Since, from Eq. (4.6), $Dn_{c0}/(\rho_0 a_0) \propto D^{1/2}A^{-1/2}$ and $a_0^2 \propto A^{2/3}$, we find that in the subleading term, $Dn_{c0}/(\rho_0 a_0)a_0^2$ is proportional to $D^{1/2}A^{1/6}$. In this way, we analytically find that, in contrast to other formulas, our formula includes the $O(A^{1/6})$ term in addition to the leading $O(A^{2/3})$ term in $\tilde{\sigma}_{\rm BS}(T_p)$. The presence of the $O(A^{1/6})$ term, which comes from the nuclear optical depth, is *one of the salient features of the present formula*.

In order to illustrate the contribution from the $O(A^{1/6})$ term, in Fig. 8, we compare the values of the BS cross-section formula (solid curve) with the values obtained by using the square-well potential within the eikonal approximation (dashed curve) for the cases of $^{\rm natu.}$C and Pb. The expression for σ_R in the eikonal approximation can be obtained from the square-well potential as Eq. (B·2) in Appendix B. In this expression, for simplicity, we do not distinguish between protons and neutrons in the target. As a result of expansion, the leading term is proportional to $A^{2/3}$, while the subleading term is proportional to $A^{1/3}$ multiplied by an A dependent exponential suppression factor as can be found in Eq. (B·8), which causes a different T_p dependence from the solid curve in each panel of Fig. 8.

By comparing the solid curves in the upper and lower panels of Fig. 8, one can see the relatively weaker T_p dependence for the case of Pb. The cross section itself grows proportional to $\sim A^{2/3}$, while the T_p-dependent term is proportional to $\sim A^{1/6}$, leading to $O(A^{-1/2})$ corrections to the $O(A^{2/3})$ term. Thus, the relative change in the cross section by T_p is suppressed. This is the reason why the slope toward a lower T_p becomes steeper for the case of C than that of Pb. The latest empirical values of σ_R [52] apparently support the presence of the T_p-dependent $O(A^{-1/2})$ corrections.

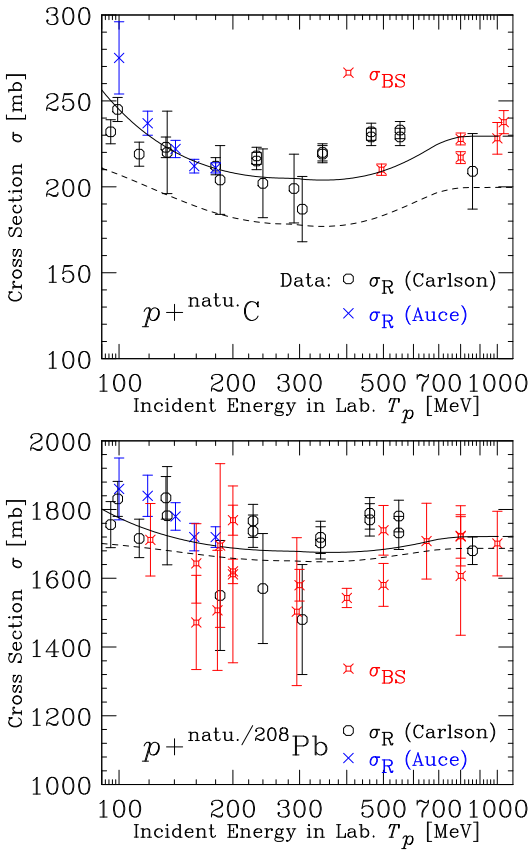

Fig. 8. (Color online) Comparison of the BS cross-section formula (solid curve) with the eikonal approximation based on the square-well potential (dashed curve) for $\sigma_R(p+^{\rm natu.}{\rm C})$ (upper) and $\sigma_R(p+^{\rm natu./208}{\rm Pb})$ (lower) as a function of the kinetic energy of an incident proton. We adopt both the BS radius at 800 MeV and the square-well radius as 2.70 fm for carbon and 7.40 fm for lead. The empirical data for σ_R and the values of $\sigma_{\rm BS}$ are the same as in Fig. 6.

Furthermore, both for C and Pb, the BS cross-section formula shows a stronger T_p dependence at $T_p \lesssim 200$ MeV than the case of the square-well potential. This is because of the different dependence of the subleading term on $\sigma_{pN}^{\rm total}$. The former is the positive power law, while the latter is the negative power law multiplied by an exponential suppression factor as in Eq. (B·2). This exponential factor drastically reduces the T_p dependence of expression (B·2), which is at odds with a power-law $\sigma_{pN}^{\rm total}$ dependence of the reaction cross section that is empirically suggested.[64]

In such conventional multiple-scattering theory as the Glauber approximation, even if one adopts a realistic density distribution as an input, a similarly weak T_p dependence of the calculated σ_R is suggested as shown in Fig. 2 of ref.[65] The influence of the surface diffuseness is secondary in this context. Therefore, a simplified comparison with our formula using the rectangular density distribution in the eikonal approximation makes sense for the purpose of clarifying the essential difference between the two approaches.

4.3 *Overestimation by the BS Cross-Section Formula at Low Energy*

At $T_p \lesssim 100$ MeV, the values of the BS cross-section formula overestimate the measured values of σ_R. We discuss this fact briefly in this subsection.

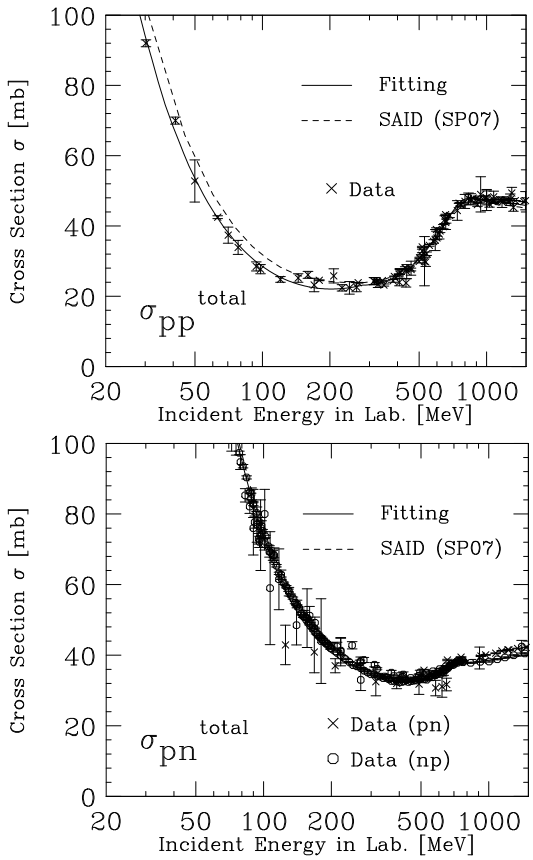

Fig. 9. The empirical values of $\sigma_{pN}^{\rm total}$ as a function of nucleon incident energies lower than 1.5 GeV. The upper panel shows $\sigma_{pp}^{\rm total}$ and the lower panel $\sigma_{pn}^{\rm total}$. These values are obtained from the compilation by the Particle Data Group.[66] What the solid and dashed curves stand for can be found in Appendix A.

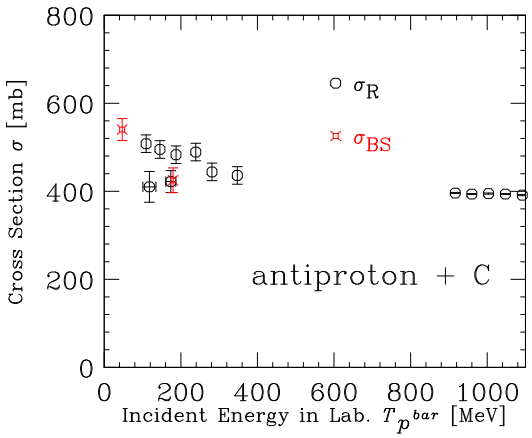

Fig. 10. (Color online) Comparison of $\sigma_{\rm BS}$ (squares with cross) with the empirical σ_R (circles) for antiproton-nucleus reactions as a function of incident kinetic energy $T_{\bar{p}}$ of antiprotons. For calculating the values of $\sigma_{\rm BS}$, we adopt the empirical values of the angular distributions for elastic scattering from ^{12}C at 46.8 MeV[69] and 179.7 MeV.[70] For comparison, we plot the empirical values of σ_R for a C target at the incident momenta of 466-879 MeV/c ($T_{\bar{p}}$ = 109.3, 145.3, 187.4, 239.0, 281.2, and 347.4 MeV) ,[72] 485 and 597 MeV/c ($T_{\bar{p}}$ = 117.9 and 173.8 MeV),[76] and 1.6-1.8 GeV/c ($T_{\bar{p}}$ = 916.6, 959.9, 1003.5, 1047.4, and 1091.6 MeV).[77] The above empirical values at $T_{\bar{p}}$ = 117.9 and 173.8 MeV are plotted with the uncertainties of around several percent in $T_{\bar{p}}$.

In constructing the formula, we assume that $|\sigma_{pN}^{\rm total} - \sigma_{pN0}^{\rm total}|$ is sufficiently small to validate $|\Delta a| \ll a_0$, which is well satisfied for $T_p \gtrsim 100$ MeV. In this sense, the overestimation by the formula simply suggests that the approximation that we adopted becomes invalid.

Let us look at which energy the value of $\sigma_{pN}^{\rm total}$ is equal to that of $T_p \simeq 800$ MeV, which we denote by $\sigma_{pN0}^{\rm total}$ in Sec. 3 of ref.[21] From Fig. 9, which plots $\sigma_{pN}^{\rm total}$ as a function of the kinetic energy of an incident nucleon, one can observe that $\sigma_{pp}^{\rm total} \simeq \sigma_{pp0}^{\rm total}$ at $T_p \simeq 50$ MeV and $\sigma_{pn}^{\rm total} \simeq \sigma_{pn0}^{\rm total}$ at $T_p \simeq 200$ MeV. Since we adopt the averaged value in the formula as shown in Eq. (4.3), the relevant quantity is $\sigma_{pN}^{\rm total}$, and $\sigma_{pN}^{\rm total} \simeq \sigma_{pN0}^{\rm total}$ at $T_p \simeq 120$ MeV for $N = Z$. Consequently, the value of the BS cross-section formula for $p + A$ around $T_p = 110$ MeV becomes the same as that of $T_p = 800$ MeV. At $T_p \sim 110$ MeV, the formula starts to deviate from the empirical values, and the deviation increases drastically as T_p decreases, because $|\sigma_{pN}^{\rm total} - \sigma_{pN0}^{\rm total}|$ becomes too large for $|\Delta a| \ll a_0$ to be satisfied.

5. Other Probes

It is natural to attempt to extend the BS approximation of nuclei to the processes of other hadronic probes such as antiprotons, pions, and kaons. Although the BS approximation is originally expected to provide a decent description of the reaction cross sections for any kind of incident particle that tends to be attenuated in nuclear interiors, whether this extension works or not is not obvious.

As a first step, in this section, we systematically analyze empirical data for antiproton elastic scattering and total reaction cross sections off stable nuclei at the incident energies of antiprotons of lower than about 1000 MeV .[67,68] We here focus on the case of antiprotons on C, because only in this case the empirical values of both the differential cross sections of elastic scattering and of σ_R are available. As in the same way as the case of proton projectiles, the values of $\sigma_{\rm BS}$ are obtained from the first peak position of the elastic scattering data. Note that we regard the empirical values of absorption cross sections as those of σ_R.

As for empirical data for the elastic differential cross sections, Garreta *et al.* measured the angular distributions for elastic scattering of antiprotons from ^{12}C at the incident kinetic energy, $T_{\bar{p}} = 46.8$ MeV,[69] and from ^{12}C, ^{40}Ca, and ^{208}Pb at $T_{\bar{p}} = 179.7$ MeV .[70] We analyze the data of ^{12}C and obtain the values of $\sigma_{\rm BS}$, which are plotted in Fig. 10. We remark in passing that in the case of proton projectiles, there are no first peaks that appear in the measured elastic differential cross sections at the same incident energies. This reflects how strongly antiprotons are attenuated in the target nucleus compared with protons.

Ashford *et al.* measured the antiproton differential cross sections on Al, Cu, and Pb for two incident momenta, 514 and 633 MeV/c, but the separation of the elastic from inelastic contributions is incomplete.[71] Therefore, we do not adopt these data for the present analyses. Incidentally, a similar type of measurements was performed by Nakamura *et al.* for the differential cross sections of elastic scattering of antiprotons on C, Al, and Cu at six beam momenta between 470 and 880 MeV/c.[72]

For completeness, we mention other empirical differential cross sections of antiprotons. Bruge *et al.* comparatively studied the elastic scattering from ^{16}O and ^{18}O isotopes at 178.4 MeV,[73] and from deuterium at 179.3 MeV.[74] Lemaire *et al.*

measured the inelastic contribution from ^{12}C and ^{18}O at 50 and 180 MeV.[75]

For comparison with $\sigma_{\rm BS}$, we plot in Fig. 10 the empirical values of σ_R, which are taken from the absorption cross section data.[72,76,77] From this figure, we find that even in the reactions involving antiprotons, the values of $\sigma_{\rm BS}$ are consistent with the empirical values of σ_R within the uncertainties although the values of σ_R are rather scattered in the region of low incident energies. These results support the relevance of the BS picture for antiprotons, while the analyses of the data for other hadronic probes are in progress.

We remark that at much higher energies, there exist various data for σ_R; for example, Denisov *et al.* measured the absorption cross sections for pions, kaons, protons, and antiprotons on Li, Be, C, Al, Cu, Sn, Pb, and U in the 6 to 60 GeV/c momentum range,[78] while Carrol *et al.* measured the absorption cross sections for pions, kaons, protons, and antiprotons on targets of Li, C, Al, Cu, Sn, and Pb at 60, 200, and 280 GeV/c.[79] These data could be of some use, but are beyond the scope of the present work.

In the energy region of interest here, the total antiproton-proton cross sections are about five times larger than $\sigma_{pp}^{\rm total}$, which implies a shorter mean-free path of an antiproton in the nuclear medium than that of a proton at the same kinetic energy. According to the results of ref.,[15] the BS radii for protons are located in the nuclear surface. Note also that the values of σ_R in Fig. 10 are four or five times larger than those of $\sigma_R(p+{}^{\rm natu.}{\rm C})$ as one can see from Figs. 6 and 8. Then, we can expect that the BS radii for antiprotons are located in a significantly outer surface region. This will open up a possibility of studying the nuclear surface structure, which would control diffractive reactions in a different way for various hadronic probes.

6. Summary and Conclusion

In this article, we have found that a novel $A^{1/6}$ dependence plays a crucial role in systematically describing the energy dependence of $\sigma_R(p+A)$ (Sec. 4.2). This finding, which is based on the BS cross-section formula constructed from a simple optical depth argument (Sec. 4.2), exhibits a clear contrast with the eikonal approximation with the square-well potential (Appendix B).

The BS approximation of nuclei can be straightforwardly extended to other hadronic probes such as neutrons, antiprotons, pions, and kaons. We have shown that the case of antiprotons works well (Sec. 5). We can expect that an antiproton is sensitive to the outer surface of nuclei than a proton, because the antiproton-nucleon total cross section is relatively large.[67] It is interesting to note the possibility that various hadronic probes of various incident energies could have the corresponding BS radii cover the whole surface region.

We can also extend the present framework to the case of nucleus-nucleus reactions.[15,17] This is essential for the analyses of experimental data of neutron-rich unstable nuclei measured or to be measured at radioactive ion beam facilities such as the RI Beam Factory of RIKEN Nishina Center.[80,81] We expect that the neutron-excess dependence of empirical $\sigma_R(A+A)$ would play an important role in deducing the density dependence of nuclear symmetry energy.[2] For description of the reactions between heavy nuclei, however, it would be essential to allow for the contribution from the Coulomb dissociation, which would require additional treatment beyond the BS approximation. Studies in such new directions are now in progress.

Recently, Horiuchi *et al*. examined the sensitivity of σ_R to the neutron-skin thickness for O, Ne, Mg, Si, S, Ca, and Ni isotopes including neutron-rich unstable nuclei by performing numerical "experiments" that adopt the Glauber approximation with the density distributions obtained from the Skyrme-Hartree-Fock method.[82] They discussed such a sensitivity in terms of the reaction radius, $a_R = \sqrt{\sigma_R/\pi}$. For the case of reactions with protons, a_R is essentially the same as the BS radius a introduced in Sec. 2. They found expressions for a_R that linearly relate a_R to the point matter radius and the skin thickness with energy dependent coefficients. Their elaborate study will offer us a great insight when we consider extension of our study toward a further neutron-rich regime.

We acknowledge T. Nakatsukasa and T. Motobayashi for constructive comments and encouragement during the course of this work, M. Lantz and K. Yazaki for invaluable suggestions and comments, H. Kondo for helpful cooperation and discussion, and the members of Hokkaido University Nuclear Reaction Data Centre (JCPRG) (http://www.jcprg.org/), particularly N. Otsuka, for kindly helping us collect various data sets. Last but not least, we thank H. Iwase, S. Hashimoto, K. Niita, and other development members of PHITS for discussion on further application of our framework. This work was supported in part by Grants-in-Aid for Scientific Research on Innovative Areas through No. 24105008 provided by MEXT.

Appendix A: Parametrizations of Proton-Nucleon Total Cross Sections

For the values of $\sigma_{pN}^{\rm total}$ in Eq. (4.4), we adopt the parametrization proposed by Bertulani and De Conti, Eqs. (1) and (2) of ref.[83] For completeness, we simply summarize their expressions in the unit of mb as follows:

$$\sigma_{pp}^{\rm total} = \begin{cases} 19.6 + 4253/T_p - 375/\sqrt{T_p} + 3.86\times10^{-2}T_p \\ \quad (\text{for } T_p < 280 \text{ MeV}) \\ 32.7 - 5.52\times10^{-2}T_p + 3.53\times10^{-7}T_p^3 \\ \quad -2.97\times10^{-10}T_p^4 \\ \quad (\text{for } 280 \text{ MeV} \le T_p < 840 \text{ MeV}) \\ 50.9 - 3.8\times10^{-3}T_p + 2.78\times10^{-7}T_p^2 \\ \quad +1.92\times10^{-15}T_p^4 \\ \quad (\text{for } 840 \text{ MeV} \le T_p \le 5 \text{ GeV}) \end{cases} \tag{A·1}$$

for proton-proton collisions, and

$$\sigma_{np}^{\rm total} = \begin{cases} 89.4 - 2025/\sqrt{T_p} + 19108/T_p - 43535/T_p^2 \\ \quad (\text{for } T_p < 300 \text{ MeV}) \\ 14.2 + 5436/T_p + 3.72\times10^{-5}T_p^2 \\ \quad -7.55\times10^{-9}T_p^3 \\ \quad (\text{for } 300 \text{ MeV} \le T_p < 700 \text{ MeV}) \\ 33.9 + 6.1\times10^{-3}T_p - 1.55\times10^{-6}T_p^2 \\ \quad +1.3\times10^{-10}T_p^3 \\ \quad (\text{for } 700 \text{ MeV} \le T_p \le 5 \text{ GeV}) \end{cases} \tag{A·2}$$

for proton-neutron collisions. Here, T_p is the kinetic energy of the projectiles in the laboratory frame in the unit of MeV. These expressions, which are constructed by χ^2 fitting in such a way as to reproduce the energy dependence of the empirical $\sigma_{pN}^{\rm total}$, are valid up to 5 GeV (see Fig. 1 in ref.[83] for details).

For comparison, we estimate $\sigma_{pN}^{\rm total}$ using the SAID program of the version "SP07".[84,85] The SAID program gives several estimations of the observables based on the partial-wave analyses of the latest compilation of nucleon-nucleon scattering data.

In Fig. 9 in Sec. 4.3, we compare the two parametrizations for $\sigma_{pN}^{\rm total}$ with the empirical values as a function of nucleon incident energies lower than 1.5 GeV. The solid curves show the fitting by Bertulani and De Conti,[83] and the dashed curves are obtained by the SAID program.

As shown in Fig. 9, the parametrization given by Eqs. (A·1) and (A·2) very well reproduces the empirical values for T_p up to $\simeq$ 1.5 GeV, except for the proton-proton scattering for the energies lower than 300 MeV in which case its deviation from the SAID parametrization is appreciable due partly to uncertainties in the empirical data. Both parametrizaitons give an almost indistinguishable prediction of the proton-nucleus total reaction cross sections via Eq. (4.4), but in this work we adopt a simpler one, namely, Eqs. (A·1) and (A·2). We remark in passing that the values of the SAID program start to rapidly deviate from the data in the downward direction beyond 1.5 GeV.

Another parametrization was proposed by Charagi and Gupta.[86] This works well for proton incident energies lower than around 300 MeV in the laboratory frame. For $\sigma_{pp}^{\rm total}$, however, the parametrization underestimates the experimental values for the energies higher than around 700 MeV up to 1000 MeV and significantly overestimates them for the energies higher than around 1000 MeV. Also for $\sigma_{pn}^{\rm total}$, the agreement with the empirical values is not good for the energies higher than 400 MeV. Therefore, we do not adopt the parametrization for the present work.

Appendix B: Scattering with a Square-Well Potential of Finite Strength

In this Appendix, we derive several expressions that characterize the scattering with a square-well potential of finite strength using various expressions that appear in Sec. 2 of ref.[21] We apply the expressions derived here to discussion of the A dependence of $\sigma_R(p+A)$ in the main text. For additional expressions for scattering amplitudes and absorption cross sections that arise from the above potential, see Sec. 5 of ref.[21]

B.1 Simple Case

Let us consider the case of a complex-valued potential of finite strength

$$V_{\rm opt}(r) = (V_0 - iW_0)\theta(\bar{a} - r), \tag{B·1}$$

where V_0 and $W_0 (> 0)$ are real constants, and $\bar{a}$ is given by $A = \rho_0(4\pi/3)\bar{a}^3$, which is generally different from the BS radius a as in Eq. (2.7) (see also Eq. (2.9) of ref.[21]). Here, for simplicity, we assume the same potential cutoff scale $\bar{a}$ for neutrons and protons. Through the phase-shift function, $\chi(b)$, defined by Eq. (2.2) of ref.,[21] we write $\sigma_{\rm abs}$, Eq. (2.8) of ref.,[21] as

$$\begin{aligned}\sigma_{\rm abs} &= 2\pi\int_0^\infty bdb\,\{1 - |\exp[i\chi(b)]|^2\} \\ &= \pi\bar{a}^2 C(\alpha)\ \ (< \pi\bar{a}^2),\end{aligned} \tag{B·2}$$

where

$$C(\alpha) = 1 - \frac{2}{\alpha^2}[1 - (\alpha+1)\exp(-\alpha)], \tag{B·3}$$

with $\alpha = 4W_0\bar{a}/v$ (see Eq. (2.81) in ref.[87]). In the limit of complete absorption ($\alpha \to \infty$), Eq. (B·2) reduces to the correct form $\pi\bar{a}^2$. An extension to the case of the different potential cutoff scales between protons and neutrons will be described in Sec. 5.2 of ref.[21]

If we apply the $t\rho$ approximation to the optical potential, we obtain

$$W_0 = \frac{1}{2}\bar{\sigma}_{pN}^{\rm total}\rho_0 v, \tag{B·4}$$

which leads to

$$\alpha = 2\bar{\sigma}_{pN}^{\rm total}\rho_0\bar{a}, \tag{B·5}$$

where $\bar{\sigma}_{pN}^{\rm total}$ is given by Eq. (4.3).

B.2 A Dependence

Here we examine the target mass-number dependence of the expression for $\sigma_{\rm abs}$ given by Eq. (B·2). Since

$$\bar{a} = \epsilon A^{1/3} \propto A^{1/3}, \tag{B·6}$$

with $\epsilon = [3/(4\pi\rho_0)]^{1/3}$, and

$$\alpha = \gamma\bar{\sigma}_{pN}^{\rm total}A^{1/3} \propto A^{1/3}, \tag{B·7}$$

with $\gamma = 2\epsilon\rho_0$, we obtain

$$\begin{aligned}\sigma_{\rm abs} &= \pi\bar{a}^2 C(\alpha) \\ &= \pi\epsilon^2 A^{2/3} C\left(\gamma\bar{\sigma}_{pN}^{\rm total}A^{1/3}\right) \\ &= \pi\epsilon^2 A^{2/3} + \frac{2\pi\epsilon^2}{\gamma\bar{\sigma}_{pN}^{\rm total}}A^{1/3}\exp\left(-\gamma\bar{\sigma}_{pN}^{\rm total}A^{1/3}\right) \\ &\quad -\frac{2\pi\epsilon^2}{\gamma^2(\bar{\sigma}_{pN}^{\rm total})^2}\left[1 - \exp\left(-\gamma\bar{\sigma}_{pN}^{\rm total}A^{1/3}\right)\right].\end{aligned} \tag{B·8}$$

Each term is ordered in powers of $A^{1/3}$ except exponential factors. The term proportional to $A^{2/3}$ is independent of energy in contrast to Carlson's formula,[49] which will be briefly summarized in Sec. 6 of ref.[21]

1) G. Placzek and H. A. Bethe, Phys. Rev. **57**, 1075 (1940).
2) K. Oyamatsu and K. Iida, Prog. Theor. Phys. **109**, 631 (2003).
3) K. Iida, K. Oyamatsu, and B. Abu-Ibrahim, Phys. Lett. **B576**, 273 (2003).
4) G. D. Alkhazov, S. L. Belostotsky, and A. A. Vorobyov, Phys. Rep. **42**, 89 (1978).
5) A. Chaumeaux, V. Layly, and R. Schaeffer, Ann. Phys. **116**, 247 (1978).
6) G. J. Igo, Rev. Mod. Phys. **50**, 523 (1978).
7) C. J. Batty, E. Friedman, H. J. Gils, and H. Rebel, Adv. Nucl. Phys. **19**, 1 (1989).
8) L. Ray, G. Hoffmann, and W.R. Coker, Phys. Rep. **212**, 223 (1992).

9) E. D. Cooper, S. Hama, B. C. Clark, and R. L. Mercer, Phys. Rev. C **47**, 297 (1993).
10) B. C. Clark, L. J. Kerr, and S. Hama, Phys. Rev. C **67**, 054605 (2003).
11) H. Sakaguchi, H. Takeda, S. Toyama, M. Itoh, A. Yamagoshi, A. Tamii, M. Yosoi, H. Akimune, I. Daito, T. Inomata, T. Noro, and Y. Hosono, Phys. Rev. C **57**, 1749 (1998).
12) J. Zenihiro, H. Sakaguchi, T. Murakami, M. Yosoi, Y. Yasuda, S. Terashima, Y. Iwao, H. Takeda, M. Itoh, H. P. Yoshida, and M. Uchida Phys. Rev. C **82**, 044611 (2010).
13) A. Kohama, K. Iida, and K. Oyamatsu, Phys. Rev. C **69**, 064316 (2004).
14) A. Kohama, K. Iida, and K. Oyamatsu, Phys. Rev. C **72**, 024602 (2005).
15) K. Iida, A. Kohama, and K. Oyamatsu, J. Phys. Soc. Japan **76**, 044201 (2007).
16) A black sphere reads as "Kurotama" in Japanese.
17) A. Kohama, K. Iida, and K. Oyamatsu, Phys. Rev. C **78**, 061601(R) (2008).
18) H. Iwase, K. Niita, and T. Nakamura, J. Nucl. Sci. Technol. **39**, 1142 (2002).
19) K. Niita, T. Sato, H. Iwase, H. Nose, H. Nakashima, and L. Sihver, Radiat. Meas. **41**, 1080 (2006).
20) A. Kohama, K. Iida, K. Oyamatsu, H. Iwase, S. Hashimoto, and K. Niita, RIKEN Accel. Prog. Rep. **46**, 55 (2012).
21) (Supplemental material) [a summary of several contents including useful expressions] is provided online.
22) The data have been retrieved from IAEA-NDS (International Atomic Energy Agency (IAEA)-Nuclear Data Service (NDS)) web site http://www-nds.iaea.org/.
23) K. Iida, S. Koide, A. Kohama, and K. Oyamatsu, Mod. Phys. Lett. **A27**, 1250020 (2012).
24) G. D. Alkhazov, I. S. Novikov, and Yu. Shabelski, Int. J. Mod. Phys. E **20**, 583 (2011).
25) I. S. Novikov and Yu. Shabelski, arXiv:1302.3930 [nucl-th].
26) J. S. Blair, Phys. Rev. **108**, 827 (1957).
27) B. Fernandez and J. S. Blair, Phys. Rev. C **1**, 523 (1970).
28) L. D. Landau and E. M. Lifshitz, *Classical Theory of Fields* (Pergamon, Oxford, 1975).
29) R. D. Amado, J. P. Dedonder, and F. Lenz, Phys. Rev. C **21**, 647 (1980).
30) A. A. Korsheninnikov, E. Yu. Nikolskii, C. A. Bertulani, S. Fukuda, T. Kobayashi, E. A. Kuzmin, S. Momota, B. G. Novatskii, A. A. Ogloblin, A. Ozawa, V. Pribora, I. Tanihata, and K. Yoshida, Nucl. Phys. **A617**, 45 (1997).
31) L. G. Votta, P. G. Roos, N. S. Chant, and R. Woody, III, Phys. Rev. C **10**, 520 (1974).
32) G. A. Moss, L. G. Greeniaus, J. M. Cameron, D. A. Hutcheon, R. L. Liljestrand, C. A. Miller, G. Roy, B. K. S. Koene, W. T. H. van Oers, A. W. Stetz, A. Willis, and N. Willis, Phys. Rev. C **21**, 1932 (1980).
33) M. Yoshimura, M. Nakamura, H. Akimune, I. Daito, T. Inomata, M. Itoh, M. Kawabata, T. Noro, H. Sakaguchi, H. Takeda, A. Tamii, K. Yonehara, H. P. Yoshida, and M. Yosoi, Phys. Rev. C **63**, 034618 (2001).
34) T. Yamagata, N. Warashina, H. Akimune, S. Asaji, M. Fujiwara, M. B. Greenfield, H. Hashimoto, R. Hayami, T. Ishida, K. Kawase, M. Kinoshita, T. Kudoh, K. Nakanishi, S. Nakayama, S. Okumura, K. Sagara, M. Tanaka, H. Utsunomiya, and M. Yosoi, Phys. Rev. C **74**, 014309 (2006).
35) J. Berger, J. Duflo, L. Goldzahl, F. Plouin, J. Oostens, M. Van Den Bossche, L. Vu Hai, G. Bizard, C. Le Brun, F. L. Fabbri, P. Picozza, and L. Satta, Phys. Rev. Lett. **37**, 1195 (1976) [Errata **37**, 1651 (1976)].
36) E. Aslanides, T. Bauer, R. Bertini, R. Beurtey, A. Boudard, F. Brochard, G. Bruge, A. Chaumeaux, H. Catz, J. M. Fontaine, R. Frascaria, D. Garreta, P. Gorodetzky, J. Guyot, F. Hibou, D. Legrand, M. Matoba, Y. Terrien, J. Thirion, and E. Lambert, Phys. Lett. **68B**, 221 (1977).
37) H. Courant, K. Einsweiler, T. Joyce, H. Kagan, Y. I. Makdisi, M. L. Marshak, B. Mossberg, E. A. Peterson, K. Ruddick, T. Walsh, G. J. Igo, R. Talaga, A. Wriekat, and R. Klem, Phys. Rev. C **19**, 104 (1979).
38) S. L. Verbeck, J. C. Fong, G. Igo, C. A. Whitten Jr., D. L. Hendrie, Y. Terrien, V. Perez-Mendez, and G. W. Hoffmann, Phys. Lett. **59B**, 339 (1975).
39) E. T. Boschitz, W. K. Roberts, J. S. Vincent, M. Blecher, K. Gotow, P. C. Gugelot, C. F. Perdrisat, L. W. Swenson, and J. R. Priest, Phys. Rev. C **6**, 457 (1972).
40) J. Fain, J. Gardes, A. Lefort, L. Meritet, J. F. Pauty, G. Peynet, M. Querrou, F. Vazeille, and B. Ille, Nucl. Phys. **A262**, 413 (1976).
41) J. Fong, T. S. Bauer, G. J. Igo, G. Pauletta, R. Ridge, R. Rolfe, J. Soukup, C. A. Whitten Jr, G. W. Hoffmann, N. Hintz, M. Oothoudt, G. Blanpied, R. L. Liljestrand, and T. Kozlowski, Phys. Lett. **B78**, 205 (1978).
42) C. B. Fulmer, J. B. Ball, A. Scott, and M. L. Whiten, Phys. Rev. **181**, 1565 (1969).
43) T. Noro, H. Sakaguchi, M. Nakamura, K. Hatanaka, F. Ohtani, H. Sakamoto, and S. Kobayashi, Nucl. Phys. **A366**, 189 (1981).
44) H. Sakaguchi, M. Nakamura, K. Hatanaka, A. Goto, T. Noro, F. Ohtani, H. Sakamoto, H. Ogawa, and S. Kobayashi, Phys. Rev. C **26**, 944 (1982).
45) K. Kwiatkowski and N. S. Wall, Nucl. Phys. **A301**, 349 (1978).
46) P. G. Roos and N. S. Wall, Phys. Rev. **140**, B1237 (1965).
47) A. Ingemarsson, T. Johansson, and G. Tibell, Nucl. Phys. **A322**, 285 (1979).
48) H. Kondo, *Master thesis*, Graduate School of Integrated Arts and Sciences, Kochi University (2013) [in Japanese].
49) R. F. Carlson, At. Data Nucl. Data Tables **63**, 93 (1996).
50) R. E. Richardson, W. P. Ball, C. E. Leith, Jr., and B. J. Moyer, Phys. Rev. **86**, 29-41 (1952).
51) E. Heiberg, Phys. Rev. **106**, 1271 (1957).
52) A. Auce, A. Ingemarsson, R. Johansson, M. Lantz, G. Tibell, R. F. Carlson, M. J. Shachno, A. A. Cowley, G. C. Hillhouse, N. M. Jacobs, J. A. Stander, J. J. van Zyl, S. V. Fortsch, J. J. Lawrie, F. D. Smit, and G. F. Steyn, Phys. Rev. C **71**, 064606 (2005).
53) P. U. Renberg, D. F. Measday, M. Pepin, P. Schwaller, B. Favier, and C. Richard-Serre, Nucl. Phys. **A183**, 81 (1972).
54) G. W. Hoffmann, M. L. Barlett, D. Ciskowski, G. Pauletta, M. Purcell, L. Ray, J. F. Amann, J. J. Jarmer, K. W. Jones, S. Penttila, N. Tanaka, M. M. Gazzaly, J. R. Comfort, B. C. Clark, and S. Hama, Phys. Rev. C **41**, 1651 (1990).
55) A. Nadasen, P. Schwandt, P. P. Singh, W. W. Jacobs, A. D. Bacher, P. T. Debevec, M. D. Kaitchuck, and J. T. Meek, Phys. Rev. C **23**, 1023 (1981).
56) W. T. H. van Oers, Huang Haw, N. E. Davison, A. Ingemarsson, B. Fagerstrom, and G. Tibell, Phys. Rev. C **10**, 307 (1974).
57) D. K. McDaniels, J. R. Tinsley, J. Lisantti, D. M. Drake, I. Bergqvist, L. W. Swenson, F. E. Bertrand, E. E. Gross, D. J. Horen, T. P. Sjoreen, R. Liljestrand, and H. Wilson, Phys. Rev. C **33**, 1943 (1986).
58) L. Lee, T. E. Drake, S. S. M. Wong, D. Frekers, R. E. Azuma, L. Buchmann, A. Galindo-Uribarri, J. D. King, R. Schubank, R. Abegg, R. Helmer, K. P. Jackson, C. A. Miller, S. Yen, and H. V. Von Geramb, Phys. Lett. **B205**, 219 (1988).
59) D. A. Hutcheon, W. C. Olsen, H. S. Sherif, R. Dymarz, J. M. Cameron, J. Johansson, P. Kitching, P. R. Liljestrand, W. J. McDonald, C. A. Miller, G. C. Neilson, D.M. Sheppard, D. K. McDaniels, J. R. Tinsley, P. Schwandt, L. W. Swenson, C. E. Stronach, Nucl. Phys. **A483**, 429 (1988).
60) G. W. Hoffmann, L. Ray, M. L. Barlett, R. Fergerson, J. McGill, E. C. Milner, Kamal K. Seth, D. Barlow, M. Bosko, S. Iverson, M. Kaletka, A. Saha, and D. Smith, Phys. Rev. Lett. **47**, 1436 (1981).
61) A. M. Mack, N. M. Hintz, D. Cook, M. A. Franey, J. Amann, M. Barlett, G. W. Hoffmann, G. Pauletta, D. Ciskowski, and M. Purcell, Phys. Rev. C **52**, 291 (1995).
62) The GEM collaboration, H. Machner and B. Razen, Nucl. Instru. Meth. **A437**, 419 (1999).
63) J. R. Letaw, R. Silberberg, and C. H. Tsao, Astrophys. J. Suppl., **51**, 271 (1983).
64) A. Ingemarsson and M. Lantz, Phys. Rev. C **72**, 064615 (2005).
65) B. Abu-Ibrahim, W. Horiuchi, A. Kohama, and Y. Suzuki, Phys. Rev. C **77**, 034607 (2008) [Errata C **80**, 029903 (2009)].
66) Particle Data Group, Phys. Rev. D **86**, 010001 (2012): Data are downloaded from http://pdg.lbl.gov/
67) A. Kohama, K. Iida, and K. Oyamatsu, RIKEN Accel. Prog. Rep. **42**, 58 (2009).
68) A. Kohama, K. Iida, and K. Oyamatsu, AIP Conf. Proc. **1355**, 115 (2011).
69) D. Garreta, P. Birien, G. Bruge, A. Chaumeaux, D. M. Drake, S. Janouin, D. Legrand, M. C. Mallet-Lemaire, B. Mayer, J. Pain, J. C. Peng, M. Berrada, J. P. Bocquet, E. Monnand, J. Mougey, P. Perrin, E. Aslanides, O. Bing, A. Erell, J. Lichtenstadt, and A. I. Yavin, Phys. Lett. **B135**, 266 (1984) [Errata **B139**, 464 (1984)].
70) D. Garreta, P. Birien, G. Bruge, A. Chaumeaux, D. M. Drake, S. Janouin, D. Legrand, M. C. Lemaire, B. Mayer, J. Pain, J. C. Peng, M. Berrada, J. P. Bocquet, E. Monnand, J. Mougey, P. Perrin, E. Aslanides, O. Bing,

J. Lichtenstadt, and A. I. Yavin, Phys. Lett. **B149**, 64 (1984); [Errata **B151**, 473 (1985)].
71) V. Ashford, M. E. Sainio, M. Sakitt, J. Skelly, R. Debbe, W. Fickinger, R. Marino, and D. K. Robinson, Phys. Rev. C **30**, 1080 (1984).
72) K. Nakamura, J. Chiba, T. Fujii, H. Iwasaki, T. Kageyama, S. Kuribayashi, T. Sumiyoshi, T. Takeda, H. Ikeda, and Y. Takada, Phys. Rev. Lett. **52**, 731 (1984).
73) G. Bruge, A. Chaumeaux, P. Birien, D. M. Drake, D. Garreta, S. Janouin, D. Legrand, M.C. Lemaire, B. Mayer, J. Pain, M. Berrada, J. P. Bocquet, E. Monnand, J. Mougey, P. Perrin, E. Aslanides, O. Bing, J. Lichtenstadt, A. I. Yavin, and J. C. Peng, Phys. Lett. **B169**, 14 (1986).
74) G. Bruge, D. Garreta, P. Birien, H. Catz, A. Chaumeaux, S. Janouin, D. Legrand, M. C. Lemaire, B. Mayer, J. Pain, F. Perrot, E. Aslanides, O. Bing, D. M. Drake, J. C. Peng, M. Berrada, J. P. Bocquet, E. Monnand, J. Mougey, P. Perrin, J. Lichtenstadt, and A. I. Yavin, Phys. Rev. C **37**, 1345 (1988).
75) M. -C. Lemaire, P. Birien, G. Bruge, D. M. Drake, D. Garreta, S. Janouin, D. Legrand, B. Mayer, J. Pain, J. C. Peng, M. Berrada, J. P. Bocquet, E. Monnand, J. Mougey, P. Perrin, E. L. Aslanides, O. Bing, J. Lichtenstadt, and A. I. Yavin, Nucl. Phys. **A456**, 557 (1986).
76) H. Aihara, J. Chiba, H. Fujii, T. Fujii, H. Iwasaki, T. Kamae, K. Nakamura, T. Sumiyoshi, Y. Takada, T. Takeda, M. Yamauchi, and H. Fukuma, Nucl. Phys. **A360**, 291 (1981).
77) R. J. Abrams, R. L. Cool, G. Giacomelli, T. F. Kycia, B. A. Leontic, K. K. Li, A. Lundby, D. N. Michael, and J. Teiger, Phys. Rev. D **4**, 3235 (1971).
78) S. P. Denisov, S. V. Donskov, Yu. P. Gorin, R. N. Krasnokutsky, A. I. Petrukhin, Yu .D. Prokoshkin, and D. A. Stoyanova, Nucl. Phys. **B61**, 62 (1973).
79) A. S. Carroll, I-H. Chiang, T. F. Kycia, K. K. Li, M. D. Marx, D. C. Rahm, W. F. Baker, D. P. Earty, G. Giacomelli, A. M. Jonckheere, P. F. M. Koehler, P. O. Mazur, R. Rubinstein, and O. Fackler, Phys. Lett. **B80**, 319 (1979).
80) A. Ozawa, T. Suzuki, and I. Tanihata, Nucl. Phys. **A693**, 32 (2001).
81) M. Takechi, T. Ohtsubo, M. Fukuda, D. Nishimura, T. Kuboki, T. Suzuki, T. Yamaguchi, A. Ozawa, T. Moriguchi, H. Ooishi, D. Nagae, H. Suzuki, S. Suzuki, T. Izumikawa, T. Sumikama, M. Ishihara, H. Geissel, N. Aoi, Rui-Jiu Chen, De-Qing Fang, N. Fukuda, I. Hachiuma, N. Inabe, Y. Ishibashi, Y. Ito, D. Kameda, T. Kubo, K. Kusaka, M. Lantz, Yu-Gang Ma, K. Matsuta, M. Mihara, Y. Miyashita, S. Momota, K. Namihira, M. Nagashima, Y. Ohkuma, T. Ohnishi, M. Ohtake, K. Ogawa, H. Sakurai, Y. Shimbara, T. Suda, and H. Takeda, S. Takeuchi, K. Tanaka, R. Watanabe, M. Winkler, Y. Yanagisawa, Y. Yasuda, K. Yoshinaga, A. Yoshida, K. Yoshida, Phys. Lett. **B707**, 357 (2012).
82) W. Horiuchi, Y. Suzuki, and T. Inakura, Phys. Rev. C **89**, 011601(R) (2014).
83) C. A. Bertulani and C. De Conti, Phys. Rev. C **81**, 064603 (2010).
84) R. A. Arndt, W. J. Briscoe, I. I. Strakovsky, and R. L. Workman, Phys. Rev. C **76**, 025209 (2007).
85) The SAID Partial-Wave Analysis Facility is based at GWU. http://gwdac.phys.gwu.edu/
86) S. K. Charagi and S. K. Gupta, Phys. Rev. C **41**, 1610 (1990).
87) Y. Suzuki, R. G. Lovas, K. Yabana, and K. Varga, *Structure and Reactions of Light Exotic Nuclei* (Taylor & Francis, London, 2003).

Supplement to "Energy and Mass-Number Dependence of Hadron-Nucleus Total Reaction Cross Sections" [J. Phys. Soc. Japan 85 (2016)]

Akihisa Kohama,[1] Kei Iida,[1,2] and Kazuhiro Oyamatsu[1,3]

[1]*RIKEN Nishina Center, RIKEN, 2-1 Hirosawa, Wako-shi, Saitama 351-0198, Japan*
[2]*Department of Natural Science, Faculty of Science, Kochi University, Kochi 780-8520, Japan*
[3]*Department of Human Informatics, Aichi Shukutoku University, 2-9 Katahira, Nagakute, Aichi, 480-1197, Japan*

We here summarize additional contents including several useful expressions. We use units in which $\hbar = c = 1$.

1. A Possible Relation to Density Distributions

In this section, we discuss where the black sphere (BS) radius, a, at $T_p \gtrsim 800$ MeV is located in the nuclear density distribution. We then compare the mass number dependence of $r_{\rm BS}$ with that of r_m.

1.1 Which Part is Probed?

Let us first define the critical nucleon density n_c as the density at $r = a$. We then deduce the values of a and n_c for ^{4}He, $^{\rm natu.}$C, ^{124}Sn, and $^{\rm natu.}$Pb from elastic scattering data at $T_p = 800$ MeV (see ref. 1 and references therein). The resultant values of n_c are listed in Table I. We find that in all the cases the BS radius is located in the surface region. We also find that n_c weakly depends on A in a manner that is consistent with $n_c \propto A^{-1/6}$. This dependence is discussed in Sec. 4 of ref. 2.

1.2 $r_{\rm BS}$ vs. r_m

In this subsection, we discuss the behavior of $r_{\rm BS} - r_m$ as a function of A at $T_p \gtrsim 800$ MeV. As we showed in ref. 3 (see Fig. 1), $r_{\rm BS} - r_m$ is consistent with zero for $A \gtrsim 50$, while $r_{\rm BS} - r_m$ is appreciably below zero for $A \lesssim 50$.

As we mentioned in ref. 3 and in Sec. 3.2 of ref. 2, the drastic change in the difference around $A \sim 50$ suggests a possible change in the form of the real nucleon density distribution; the rectangular distribution as assumed in deducing the rms radius $r_{\rm BS}$ may well simulate the real distribution at $A \gtrsim 50$, while for $A \lesssim 50$ the real distribution is quite different from the rectangular one in such a way that the portion of the real distribution farther than a is relatively large. This feature is suggested by the empirical charge distribution deduced from the electron-nucleus elastic scattering,[4] which shows a Gaussian-like form rather than a rectangular one for light nuclei.

This feature of the nucleon distribution is expected to be reflected by size-sensitive observables for which empirical data are available for stable nuclei ranging from light to heavy ones. Such observables include $1s$ states of pionic atoms and isoscalar giant resonance energies; the isoscalar part of the pion-nucleus optical potential[5] and the inertia associated with the resonances[6] are related to the nucleon distribution.

Table I. The values of n_c at $T_p = 800$ MeV.

Nucleus	n_c (fm^{-3})
$^{\rm natu.}$Pb	0.028
^{124}Sn	0.033
$^{\rm natu.}$C	0.044
^{4}He	0.060

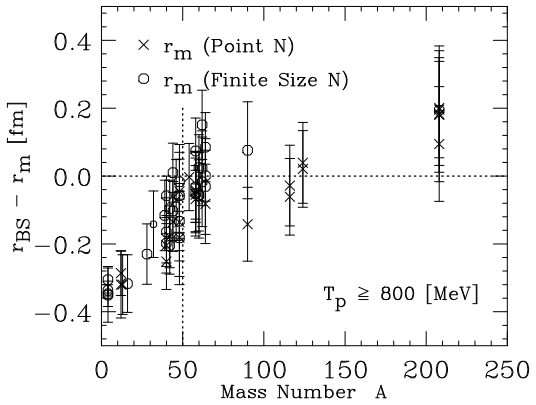

Fig. 1. The difference, $r_{\rm BS} - r_m$, as a function of mass number A (from Fig. 2 of ref. 3). The crosses (×) and the circles (○) are calculated from the corresponding values of r_m in Fig. 1 of ref. 3. The dotted line shows $r_{\rm BS} = r_m$ and $A = 50$.

To make the problem clearer, we adopt the two-parameter Fermi function as a typical nuclear density distribution. By expanding it in terms of $A^{1/3}$, we obtain the rms radius as (see Eq. (2-71) in p. 161 of ref. 7)

$$\langle r^2 \rangle^{1/2} = 0.93A^{1/3} + 1.78A^{-1/3} + \cdots \text{ fm}. \qquad (1.1)$$

From the above expression, we can understand that the first term of the right side corresponds basically to the BS scaling of $r_{\rm BS} = 0.94A^{1/3}$ fm, Eq. (3.3) of ref. 2. A part of the difference for $A \lesssim 50$ found in Fig. 1 comes from the second term of Eq. (1.1). A more systematic study in this direction was reported in ref. 8 (see also Sec. 4 in this supplement).

2. Connection with the Eikonal Approximation

In this section, we show the connection of our BS approximation of nuclei with the eikonal approximation, and summarize the key expressions for the purpose of completeness and clarification.

The scattering amplitude of proton-nucleus elastic scatter-

ing, $f(\mathbf{q})$, in the eikonal approximation is given by[9)]

$$f(\mathbf{q}) = ip \int_0^\infty bdb\ J_0(qb)\{1 - \exp[i\chi(b)]\}, \tag{2.1}$$

where $\mathbf{q}$ is the momentum transfer, $\mathbf{p}$ is the proton momentum in the c.m. frame, $\mathbf{b}$ is the impact parameter vector perpendicular to $\mathbf{p}$, $J_n(x)$ is the n-th order Bessel function, and

$$\chi(\mathbf{b}) = -\frac{1}{v}\int_{-\infty}^{\infty} dz'\ V_{\rm opt}(\mathbf{b} + \kappa z'), \tag{2.2}$$

is the phase-shift function with the velocity of an incident proton $v\left(= |\mathbf{p}|/\sqrt{\mathbf{p}^2 + m_p^2}\right)$, the proton-nucleus optical potential $V_{\rm opt}(\mathbf{r})$, and $\kappa = \mathbf{p}/|\mathbf{p}|$. We then obtain the differential cross section of elastic scattering as

$$\frac{d\sigma_{\rm elastic}}{d\Omega} = |f(\mathbf{q})|^2. \tag{2.3}$$

Within the $t\rho$ approximation to the optical potential,[9)] the phase-shift function reads

$$\chi(b) = \frac{2\pi}{p}\sum_{N=n,p} f_{pN}(\mathbf{0})\int_{-\infty}^{\infty} dz'\ \rho_N(\mathbf{b} + \kappa z'), \tag{2.4}$$

where $f_{pN}(\mathbf{0})$ is the proton-nucleon scattering amplitude in the forward direction, and $\rho_N(\mathbf{r})$ is the N nucleon one-body density distribution. Expression (2.4) corresponds to the optical-limit approximation in the Glauber approximation. The imaginary part of $f_{pN}(\mathbf{0})$ is related to $\sigma_{pN}^{\rm total}$ by the optical theorem as

$$\mathrm{Im} f_{\rm pN}(\mathbf{0}) = \frac{p}{4\pi}\sigma_{pN}^{\rm total}. \tag{2.5}$$

Using the scattering amplitude of Eq. (2.1) in the forward direction, we obtain the total cross section via the optical theorem for proton-nucleus scattering as

$$\begin{aligned}\sigma_{\rm total} &= \frac{4\pi}{p}\mathrm{Im} f(\mathbf{0}) \\ &= 4\pi\int_0^\infty bdb\ \{1 - \mathrm{Re}\ \exp[i\chi(b)]\}.\end{aligned} \tag{2.6}$$

Note that this allows for the contribution from the strong interaction alone. The total elastic scattering cross section can be obtained from Eq. (2.3) as

$$\sigma_{\rm elastic} = 2\pi\int_0^\infty bdb\ |\exp[i\chi(b)] - 1|^2, \tag{2.7}$$

which in turn leads to the absorption cross section,

$$\begin{aligned}\sigma_{\rm abs} &= \sigma_{\rm total} - \sigma_{\rm elastic} \\ &= 2\pi\int_0^\infty bdb\ \{1 - |\exp[i\chi(b)]|^2\} \\ &= 2\pi\int_0^\infty bdb\ \{1 - \exp[-2\mathrm{Im}\chi(b)]\}.\end{aligned} \tag{2.8}$$

In the strongly absorptive limit of the eikonal approximation with the density distribution whose cutoff is equal to the BS radius a, we can write the phase-shift function, $\chi(b)$, as

$$\exp[i\chi(b)] = \theta(b - a). \tag{2.9}$$

Then, the scattering amplitude becomes the Fraunhofer scattering amplitude in optics:

$$f(\mathbf{q}) = ipaJ_1(qa)/q. \tag{2.10}$$

Using expression (2.9), we obtain from Eq. (2.6)

$$\sigma_{\rm total} = 2\pi a^2. \tag{2.11}$$

Also, we obtain

$$\sigma_{\rm elastic} = \pi a^2 \tag{2.12}$$

and

$$\sigma_{\rm abs} = \pi a^2. \tag{2.13}$$

In this framework, the absorption cross section $\sigma_{\rm abs}$ corresponds to the BS cross section $\sigma_{\rm BS} = \pi a^2$ and thus can be identified with the total reaction cross section σ_R of proton-nucleus scattering. This is the formal relation of the BS approximation with the eikonal approximation.

As described in Sec. 2.2 of ref. 2, we determine a by fitting the angle of the first elastic diffraction peak calculated for proton diffraction by a circular black disk of radius a to the measured value, which is the essential difference from the classical BS approximation.

3. Derivation of the BS Cross-Section Formula

In this section, we describe how to derive the BS cross-section formula. This formula was originally reported in ref. 10. The present description is partly a repetition of that work, but aims at being more detailed.

We express the energy dependence of $\sigma_{\rm BS}$ ($\equiv \pi a^2$), Eq. (2.8) of ref. 2, as

$$\begin{aligned}\tilde{\sigma}_{\rm BS}(T_p) &= \pi a(T_p)^2 \\ &= \pi a_0^2\left(1 + \frac{\Delta a}{a_0}\right)^2,\end{aligned} \tag{3.1}$$

where $\Delta a \equiv a(T_p) - a_0$ is responsible for the energy dependence of $\tilde{\sigma}_{\rm BS}$. a_0 is the value of a determined at 800 MeV in the same way as in Sec. 2.2 of ref. 2. In this setting, we assume that the incident protons are point particles, leading to vanishing contribution from the proton size to a. This is reasonable since the measured proton-proton reaction cross section is relatively small at T_p less than $\sim$ 1000 MeV.

In deriving the expression for Δa, we introduce the "optical" depth or thickness of a target nucleus. As originally introduced in astrophysics,[11)] the optical depth, or optical thickness, is a measure of transparency and is defined as the negative logarithm of the fraction of radiation that is not scattered or absorbed on a path. In the present "optical" depth, we consider the fraction of projectiles that are transparent through the target nucleus, because the BS radius a corresponds to a critical radius inside which the protons are attenuated in a target nucleus.

In the context of the conventional nuclear scattering theory, as one can see from expression (2.8), the fraction is in proportion to the flux attenuation factor, which can be obtained from $\mathrm{Im}\,\chi(b)$, Eq. (2.4), as

$$\begin{aligned}|\exp[\chi(b)]|^2 &= \exp[-2\mathrm{Im}\chi(b)] \\ &= \exp\left[-\sum_{N=n,p}\sigma_{pN}^{\rm total}\int_{-\infty}^{\infty} dz'\ \rho_N(\mathbf{b} + \kappa z')\right].\end{aligned} \tag{3.2}$$

Thus, the nuclear optical depth for absorption of proton pro-

jectiles in the conventional scattering theory can be symbolically expressed as

$$\tau_{\rm conv} = \int_l dl \left[\sigma_{pn}^{\rm total}\rho_n(\mathbf{r}) + \sigma_{pp}^{\rm total}\rho_p(\mathbf{r})\right], \tag{3.3}$$

where l is the proton trajectory.

The empirical relation that $\sigma_R \simeq \sigma_{\rm BS}$ suggests that expression (3.3) amounts to a critical value when the nearest distance between the proton trajectory and the nuclear center is a. Let us now approximate the trajectory by a straight line (Fig. 5 of ref. 2) although it is slightly distorted by the Coulomb repulsion.

In the present framework, instead of Eq. (3.3), we introduce the *effective* nuclear optical depth τ, Eq. (4.2) of ref. 2. By approximating the nuclear density distribution as a trapezoidal form as shown in Fig. 5 of ref. 2, we express L' by

$$L' = 2\sqrt{R^2 - a^2}. \tag{3.4}$$

In the trapezoidal form of the nucleon distributions, we set the length of the bottom, R, the surface thickness, D, and the length of the top, $R-D$, in such a way as to reproduce a typical behavior of the distributions deduced from elastic scattering data off stable nuclei. The surface thickness D is the thickness outside of the plateau of the density distribution of density ρ_0.

Let us now consider the deviation of ΔX of X ($= \bar\sigma_{pN}^{\rm total}, a, n_c,$ and L') from the value X_0 at $T_p = 800$ MeV under the condition that the nuclear optical depth τ is independent of T_p. As long as $T_p > 100$ MeV, $\Delta\bar\sigma_{pN}[= \bar\sigma_{pN}^{\rm total}(T_p) - \bar\sigma_{pN0}^{\rm total}]$ is sufficiently small to validate the following expression up to first order in the deviations

$$\tau\frac{\Delta\bar\sigma_{pN}^{\rm total}}{(\bar\sigma_{pN0}^{\rm total})^2} \approx -n_{c0}\Delta L' - L_0'\Delta n_c, \tag{3.5}$$

which follows from

$$\Delta\left(\frac{\tau}{\bar\sigma_{pN}^{\rm total}}\right) = \Delta(n_c L'). \tag{3.6}$$

$\Delta L'$ in Eq. (3.5) can be rewritten as

$$\Delta L' \approx \left.\frac{dL'}{da}\right|_0 \Delta a. \tag{3.7}$$

Because of the assumed trapezoidal distribution, one can obtain

$$\Delta n_c = -\frac{\rho_0}{D}\Delta a. \tag{3.8}$$

For the estimation of D, we consider the slope to be linear near the half-density radius as the simplest approximation. For example, as the nuclear density distribution $\sum_{N=n,p}\rho_N(\mathbf{r})$, we adopt the two-parameter Fermi distribution,

$$\rho_{\rm 2pF}(r) = \frac{\rho_{f0}}{1+\exp{(r-c)/z}}, \tag{3.9}$$

where c is the half-density radius, and z determines the diffuseness. Typically, they are parameterized as $c \simeq 1.3A^{1/3}$ fm and $z \simeq 0.5$ fm, respectively. The condition that the slope should be the same at $r = c$ reads

$$\left.\frac{d\rho_{\rm 2pF}(r)}{dr}\right|_{r=c} = -\rho_{f0}\frac{1}{4z} = \frac{\rho_0}{D}. \tag{3.10}$$

Assuming $\rho_{f0} \simeq \rho_0$, we obtain $D = 4z$. The value of $z = 0.55$ fm corresponds to $D = 2.2$ fm, which is taken throughout the present work.

Combining Eqs. (3.5), (3.7), and (3.8), one can derive the relation between $\Delta\bar\sigma_{pN}$ and Δa as

$$\begin{aligned}\frac{\Delta a}{a_0} &= \left(\frac{\rho_0}{D}L_0' - \left.\frac{dL'}{da}\right|_0 n_{c0}\right)^{-1}\frac{\tau}{a_0}\frac{\Delta\bar\sigma_{pN}^{\rm total}}{(\bar\sigma_{pN0}^{\rm total})^2} \\ &= \left(\frac{\rho_0 a_0}{Dn_{c0}} - \frac{a_0}{L_0'}\left.\frac{dL'}{da}\right|_0\right)^{-1}\frac{\Delta\bar\sigma_{pN}^{\rm total}}{\bar\sigma_{pN0}^{\rm total}}.\end{aligned} \tag{3.11}$$

We thus obtain the BS cross-section formula as

$$\tilde\sigma_{\rm BS}(T_p) = \pi a_0^2\left[1 + \left(\frac{\rho_0 a_0}{Dn_{c0}} - \frac{a_0}{L_0'}\left.\frac{dL'}{da}\right|_0\right)^{-1}\frac{\Delta\bar\sigma_{pN}^{\rm total}}{\bar\sigma_{pN0}^{\rm total}}\right]^2, \tag{3.12}$$

where $L_0' = 2\sqrt{R^2 - a_0^2}$, $\rho_0 = 0.16$ fm^{-3}, and n_{c0} is given by

$$n_{c0} = \tau/(L_0'\bar\sigma_{pN0}^{\rm total}). \tag{3.13}$$

Here we choose $\tau = 0.9$ in such a way as to reproduce the values of n_{c0} that are summarized in Table I in Sec. 1. For $\sigma_{pp}^{\rm total}$ and $\sigma_{pn}^{\rm total}$, see Appendix A of ref. 2.

We now proceed to express dL'/da at $T_p = 800$ MeV and the length R. In doing so, we first note the normalization condition for the assumed trapezoidal distribution,

$$A = \frac{4\pi\rho_0}{3}\left(R^3 - \frac{3}{2}DR^2 + D^2R - \frac{1}{4}D^3\right). \tag{3.14}$$

While we could solve this in R analytically, we solve it approximately for later convenience. One can seek an approximate solution to Eq. (3.14) by setting

$$R = R_0 + D/2 + \delta R, \tag{3.15}$$

with

$$R_0 = [3A/(4\pi\rho_0)]^{1/3}, \tag{3.16}$$

and assuming that δR is small. One thus obtains

$$R \simeq R_0 + \frac{D}{2} - R_0\left(1 + \frac{12R_0^2}{D^2}\right)^{-1}. \tag{3.17}$$

From this expression, δR can be shown to be small even for light elements. Hereafter we substitute expression (3.17) into the cross-section formula (3.12) through L'.

We can then obtain dL'/da from Eqs. (3.4) and (3.17). The expression for dL'/da is given by

$$\begin{aligned}\frac{dL'}{da} &= \frac{2}{L'}\frac{d}{da}(R^2 - a^2) \\ &= \frac{4}{L'}(R\frac{dR}{da} - a).\end{aligned} \tag{3.18}$$

Since $dR/da = 0$, we can estimate the values of dL'/da at $T_p = 800$ MeV in Eq. (3.12) from

$$\left.\frac{dL'}{da}\right|_0 = -\frac{4}{L_0'}a_0. \tag{3.19}$$

Note that in our previous paper,[10] we have mistakenly assumed $dR_0/da|_0 = R_0/a_0$ in calculating $dL'/da|_0$. The relevant corrections, which are included in Eq. (3.19), act to decrease the magnitude of Δa, but change the value of $\tilde\sigma_{\rm BS}(T_p)$ by an amount of the order of typical experimental error bars

at most.

4. Comparison between Various Radii of Stable Nuclei

In this section, we briefly review ref. 8, which explains the physics underlying the fact that the A dependence of the difference between the rms BS radius $r_{\rm BS}$ and matter radius r_m of stable nuclei changes abruptly around $A = 50$ as shown in Fig. 1. In ref. 8, the author concluded that this abrupt change stems from the combined effects of the surface diffuseness and neutron skin.

Let us now recall that the BS radius a behaves almost completely as $A^{1/3}$ [3] [see Eq. (3.3) of ref. 2]. We thus find that the abrupt change of the A dependence of $r_{\rm BS} - r_m$ is controlled by r_m. To see the A dependence of r_m, we consider the rms charge radius r_c as a reference. This is because r_c is empirically well-known,[4] leading to various formulas as function of A.[12] For example, one can approximate the charge density distribution by the two-parameter Fermi distribution, leading to expansion with respect to A like Eq. (1.1). Instead, we here use the trapezoidal charge density distribution, which allows us to analytically obtain the rms charge radii. In fact, by assuming that the proton point density distribution is proportional to the trapezoidal matter density distribution given in Sec. 3 in this supplement, we obtain

$$r_c^t = \left[\frac{3}{5R_0^3}\left(3R^3 - \frac{15}{2}DR^4 + 10D^2R^3 - \frac{15}{2}D^3R^2 + 3D^4R - \frac{1}{2}D^5\right) + \frac{3}{2}r_p^2\right]^{1/2}, \tag{4.1}$$

where R_0 and R are given by Eqs. (3.16) and (3.17), respectively, and $r_p = 0.65$ fm allows for the proton charge radius.[13] Note that this expression well reproduces the overall empirical data for r_c.

We proceed to compare $r_{\rm BS}$, $\tilde{r}_m$, and r_c for stable nuclei. In Fig. 2 we plot $\tilde{r}_m - r_{\rm BS}$, where $\tilde{r}_m$ is deduced from the experimental overall differential cross sections for proton elastic scattering via optical potential models, and $r_{\rm BS}$ is obtained from the measured peak angles in the same differential cross sections. The data are the same as in Fig. 1, but here for the data for r_m that have the nucleon size ignored, we reevaluate it as $\tilde{r}_m^2$ by adding $(3/2)r_p^2$ to the original r_m^2 for the sake of consistency with the definition of r_c. For comparison, we also plot $r_c - r_{\rm BS}$, where r_c is taken from ref. 4, together with $r_c^t - 0.94A^{1/3}$ fm. As can be seen from the figure, $r_c^t - 0.94A^{1/3}$ fm well simulates the empirical behavior of $r_c - r_{\rm BS}$. For $A \lesssim 50$, $\tilde{r}_m - r_{\rm BS}$ is positive and decreases with A, a feature that comes from the contribution of the surface diffuseness to $\tilde{r}_m$. We remark that in this region, r_c is almost indistinguishable from $\tilde{r}_m$, and that the nuclear surface occupies a large portion of the density distribution for light nuclei. For $A \gtrsim 50$, on the other hand, $\tilde{r}_m - r_{\rm BS}$ is consistent with zero, while $\tilde{r}_m$ is systematically larger than r_c. The latter feature almost certainly originates from the neutron skin thickness r_{np}, i.e., the difference in the rms radius between the neutron and proton density distributions, which develops as the beta stability line deviates from $Z = A/2$ into a neutron-rich regime. In fact, $\tilde{r}_m - r_c \approx (1 - Z/A)r_{np}$.

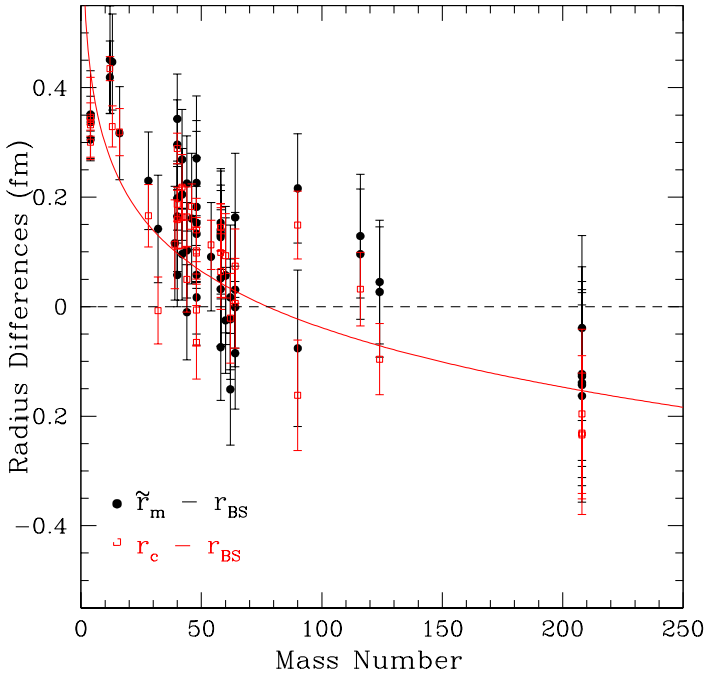

Fig. 2. (Color online) Empirical radius differences, $\tilde{r}_m - r_{\rm BS}$ (circles) and $r_c - r_{\rm BS}$ (squares), obtained for stable nuclei. The data for $\tilde{r}_m$ and $r_{\rm BS}$ adopted here are the same as in Fig. 1, but here the nucleon size is included for any $\tilde{r}_m$. For comparison, we plot $r_c^t - 0.94A^{1/3}$ fm in solid curve.

5. Supplementary Information for Appendix B: Scattering with a Square-Well Potential of Finite Strength

We here give additional expressions for scattering amplitudes and absorption cross sections that arise from the potential (B.1) of ref. 2.

5.1 *Scattering Amplitude*

Let us consider the derivation of the analytic expression for the scattering amplitude. From Eq. (2.1), we obtain

$$\begin{aligned} f(\mathbf{q}) &= ip\int_0^{\bar{a}} bdb\, J_0(qb) \times\left\{1 - \exp\left[-\frac{2(W_0 + iV_0)}{v}\sqrt{\bar{a}^2 - b^2}\right]\right\} \\ &= ip\int_0^{\bar{a}} xdx\, J_0\left(q\sqrt{\bar{a}^2 - x^2}\right) \times\{1 - \exp[-2(c_2 + ic_1)x]\} \\ &= ip(I_0 - I_c + iI_s), \end{aligned} \tag{5.2}$$

with $x = \sqrt{\bar{a}^2 - b^2}$, $c_1 = V_0/v$, $c_2 = W_0/v$,

$$I_0 = \int_0^{\bar{a}} xdx\, J_0\left(q\sqrt{\bar{a}^2 - x^2}\right) \tag{5.3}$$

$$\begin{aligned} I_c &= \int_0^{\bar{a}} xdx\, J_0\left(q\sqrt{\bar{a}^2 - x^2}\right) e^{-2c_2x}\cos(2c_1x) \\ &= -\frac{1}{2}\,{\rm Re}\frac{\partial}{\partial c_2} I_g, \end{aligned} \tag{5.4}$$

$$I_s = \int_0^{\bar{a}} xdx\, J_0\left(q\sqrt{\bar{a}^2 - x^2}\right) e^{-2c_2x}\sin(2c_1x)$$

$$= -\frac{1}{2}\,\mathrm{Im}\frac{\partial}{\partial c_2} I_g, \tag{5.5}$$

where

$$I_g = \int_0^{\bar{a}} dx\, J_0\left(q\sqrt{\bar{a}^2 - x^2}\right) \exp[-2(c_2 + ic_1)x]. \tag{5.6}$$

5.2 *Effect of Neutron Skin*

For future research involved, it could be significant to approach unstable neutron-rich nuclei. We thus extend the eikonal approximation based on the potential (B.1) of ref. 2 to the case of $a_n > a_p$, where a_n and a_p are the potential cut-off scales for neutrons and protons, respectively, as done in ref. 14. For simplicity, we confine ourselves to the case of $(a_n - a_p)/a_n \ll 1$. In this case, as we shall see, the reaction cross section (B.2) of ref. 2 includes a term that depends exponentially on the effective neutron skin thickness $a_n - a_p$.

Let us set the radius and density of the proton (neutron) distribution for a nucleus of given A and Z to be the same as a_p (a_n) and uniform at $\rho_{p0} = 3Z/(4\pi a_p^3)$ ($\rho_{n0} = 3(A-Z)/(4\pi a_n^3)$). Within the $t\rho$ approximation to the optical potential, the phase-shift function $\chi(b)$ given by Eq. (2.2) can be decomposed into

$$\chi(b) = \chi_{pp}(b) + \chi_{pn}(b), \tag{5.7}$$

where the imaginary part can be expressed as

$$\begin{aligned}\mathrm{Im}[\chi_{pp}(b) + \chi_{pn}(b)] &= \sigma_{pp}^{\mathrm{total}}\rho_{p0}\sqrt{a_p^2 - b^2}\,\theta(a_p - b) \\ &+ \sigma_{pn}^{\mathrm{total}}\rho_{n0}\sqrt{a_n^2 - b^2}\,\theta(a_n - b).\end{aligned} \tag{5.8}$$

By substitute Eq. (5.8) into Eq. (2.8), we obtain

$$\begin{aligned}\sigma_{\mathrm{abs}} &= \pi a_n^2 \\ &\quad -2\pi\int_0^{a_p} bdb\exp[-\zeta_p\sqrt{a_p^2 - b^2} \\ &\qquad -\zeta_n\sqrt{a_n^2 - b^2}] \\ &\quad -2\pi\int_{a_p}^{a_n} bdb\exp[-\zeta_n\sqrt{a_n^2 - b^2}]\end{aligned} \tag{5.9}$$

where $\zeta_p = 2\sigma_{pp}^{\mathrm{total}}\rho_{p0}$ and $\zeta_n = 2\sigma_{pn}^{\mathrm{total}}\rho_{n0}$. For later convenience, we define

$$\bar{\zeta} = \zeta_p + \zeta_n \tag{5.10}$$

In Eq. (5.9), we refer to minus the second term as (I) and to minus the third term as (II).

Since it is hard to analytically calculate (I), we will estimate the upper and lower limits of (I). Putting $y = a_p^2$ and $y_0 = a_n^2$, as well as keeping a_p and a_n being close in mind, via the mean-value theorem, we can write

$$\begin{aligned}f(y) &= \sqrt{y - b^2} \\ &= f(y_0) + f'(y_0 + c(y - y_0))(y - y_0),\end{aligned} \tag{5.11}$$

where $f' = df/dy$, and c is a number that satisfies $0 < c < 1$, while depending on b. The second term of Eq. (5.11) satisfies the following inequalities:

$$\begin{aligned}f'(y_0 + c(y - y_0)) &= \frac{1}{2\sqrt{y_0 + c(y - y_0) - b^2}} \\ &= \frac{1}{2\sqrt{(1-c)y_0 + cy - b^2}} \\ &< \frac{1}{2\sqrt{(1-c)(y_0 - y)}} \\ &< \frac{1}{\sqrt{y_0 - y}}.\end{aligned} \tag{5.12}$$

For the first inequality, we use the relation, $cy - b^2 \geq cy - y$ for $0 \leq b \leq a_p$. For the last inequality, we refer to the range of c as a function of b as shown in Table II. Then, Eq. (5.11) becomes

$$\sqrt{a_p^2 - b^2} > \sqrt{a_n^2 - b^2} - \sqrt{a_n^2 - a_p^2}, \tag{5.13}$$

and we can obtain in the case of strong absorption

$$\begin{aligned}\mathrm{(I)} &\ll 2\pi\int_0^{a_p} bdb\exp\left(-\bar{\zeta}\sqrt{a_n^2 - b^2} + \zeta_p\sqrt{a_n^2 - a_p^2}\right) \\ &= \exp\left(\zeta_p\sqrt{a_n^2 - a_p^2}\right) \\ &\quad \times 2\pi\int_0^{a_p} bdb\exp\left(-\bar{\zeta}\sqrt{a_n^2 - b^2}\right),\end{aligned} \tag{5.14}$$

where $\ll$ means that the left side is exponentially smaller than the right side.

Changing the variable of integration via $x = \sqrt{a_n^2 - b^2}$ ($xdx = -bdb$), we rewrite Eq. (5.14) as

$$\begin{aligned}\mathrm{(I)} &\ll \exp\left(\zeta_p\sqrt{a_n^2 - a_p^2}\right) \\ &\quad \times 2\pi\int_{\sqrt{a_n^2 - a_p^2}}^{a_n} xdx\exp(-\bar{\zeta}x).\end{aligned} \tag{5.15}$$

Then we can analytically calculate the integration in Eq. (5.15) using

$$\begin{aligned}\int_0^a xdx\ \exp(-bx) &= (1/b^2)[1 - (ab+1)\exp(-ab)], \\ &\quad (a, b > 0).\end{aligned} \tag{5.16}$$

The result is

$$\begin{aligned}&2\pi\int_{\sqrt{a_n^2 - a_p^2}}^{a_n} xdx\exp(-\bar{\zeta}x) \\ &= \frac{2\pi}{\bar{\zeta}^2}\left[1 - (a_n\bar{\zeta} + 1)\exp(-a_n\bar{\zeta})\right] \\ &\quad -\frac{2\pi}{\bar{\zeta}^2}\left[1 - \left(\bar{\zeta}\sqrt{a_n^2 - a_p^2} + 1\right)\exp\left(-\bar{\zeta}\sqrt{a_n^2 - a_p^2}\right)\right]. \\ &= \frac{2\pi}{\bar{\zeta}^2}\left(\bar{\zeta}\sqrt{a_n^2 - a_p^2} + 1\right)\exp\left(-\bar{\zeta}\sqrt{a_n^2 - a_p^2}\right)\end{aligned}$$

Table II. The behavior of c as a function of b.

b	0		a_p
$c(b)$	$(3a_n + a_p)/[4(a_n + a_p)]$	↗	3/4

$$-\frac{2\pi}{\bar{\zeta}^2}(a_n\bar{\zeta}+1)\exp\left(-a_n\bar{\zeta}\right). \tag{5.17}$$

In the same way as above, on the other hand, we can rewrite (II) as

$$\begin{aligned}(\mathrm{II}) &= 2\pi\int_{a_p}^{a_n} bdb\exp\left(-\zeta_n\sqrt{a_n^2-b^2}\right)\\ &= 2\pi\int_0^{\sqrt{a_n^2-a_p^2}} xdx\exp(-\zeta_n x)\\ &= \frac{2\pi}{\zeta_n^2}\left[1-(\zeta_n\sqrt{a_n^2-a_p^2}+1)\exp\left(-\zeta_n\sqrt{a_n^2-a_p^2}\right)\right].\end{aligned} \tag{5.18}$$

When one retains corrections to the BS limit ($\sigma_{pN}^{\mathrm{tot}}\to\infty$) by transparency of the skin region, (I) is negligible compared with (II). Thus, the absorption cross section (5.9) has a form

$$\begin{aligned}\sigma_{\mathrm{abs}} &\simeq \pi a_n^2\\ &\quad -\frac{2\pi}{\zeta_n^2}\left[1-\left(1+\zeta_n\sqrt{a_n^2-a_p^2}\right)e^{-\zeta_n\sqrt{a_n^2-a_p^2}}\right]\\ &\leq \pi a_n^2.\end{aligned} \tag{5.19}$$

It is instructive to note that Eq. (5.19) reduces to πa_n^2 in the BS limit. For large but finite values of ζ_n, the remaining term in the right side of Eq. (5.19) starts to play a role ahead of the other terms responsible for transparency of the inner region in which protons are present. Interestingly, this term is a decreasing function of a_n and in some cases acts to cancel an increase of the main term πa_n^2 by an increment of a_n.[14]

6. Empirical Formulas for σ_R

Here, we summarize earlier empirical formulas for σ_R of proton-nucleus reactions, some of which are plotted in Fig. 7 of ref. 2. Since the advent of the geometrical cross section formula designed for collisions of heavy cosmic ray primaries with target nuclei by Bradt and Peters,[15] several formulas have been developed mainly for description of intermediate energy nucleus-nucleus collisions. Kox *et al.* proposed a geometrical formula that expresses σ_R in powers of $A^{1/3}$ by including an energy dependent parameter obtained phenomenologically in the energy range from 30 MeV/nucleon to 2100 MeV/nucleon.[16] The expression for the energy dependent parameter as obtained above was given by Townsend and Wilson.[17] Shen *et al.* extended the formula by Kox *et al*. by taking into account the effect of neutron excess and decreasing the lower limit of its applicable energy range down to a few MeV/nucleon.[18] Tripathi *et al.* further improved the formula by introducing the "medium effect".[19,20] It should be noted that the effect of neutron excess adopted in the last two formulas leads to asymmetry with respect to exchange between projectile and target nuclei.[21]

On the basis of the formula by Bradt and Peters,[15] on the other hand, Sihver *et al.* developed semi-empirical formulas for proton-nucleus (with the target charge $Z_t \leq 26$) and nucleus-nucleus (with the projectile and target charges $Z_p, Z_t \leq 26$) reactions.[22] These formulas are applicable for incident energies above $\simeq$ 15 MeV and $\simeq$ 100 MeV/nucleon, respectively.

There is another genealogy of geometrical formulas for proton-nucleus reaction cross sections. Carlson constructed a formula that is based on a simple geometrical picture by determining the energy-dependent coefficients from empirical data of stable nuclei.[23] The values of these coefficients were parameterized by Machner *et al*.[24] Even earlier than that, a similar empirical formula was constructed for various ion-transport problems of astrophysical interest by Letaw *et al.*[25] Details of these two formulas are given below.

6.1 Carlson's Formula

The expression is given by

$$\sigma_R = \pi\left(R_p + r_0 A^{1/3}\right)^2. \tag{6.1}$$

The values of the coefficients are summarized in Table A of ref. 23. This expression includes an $A^{1/3}$ correction in addition to the simple geometrical $A^{2/3}$ term. Carlson determined this correction in such a way as to reproduce the empirical total reaction cross sections of stable nuclei colliding with protons in the energy range from 40 MeV to 560 MeV.

Machner *et al*. proposed the parametrization of R_p and r_0 as a function of the proton incident energy T_p as in Eqs. (5) and (6) of ref. 24:

$$R_p(T_p) = -0.37 + 5.538\exp(-0.0366T_p), \tag{6.2}$$

and

$$r_0(T_p) = \frac{1}{0.732 + 167.7/T_p^2}, \tag{6.3}$$

with both parameters measured in fm and the energy T_p in MeV. Expression (6.2) overestimates R_p of Eq. (6.1) between $40 \leq T_p \leq 100$ MeV.

6.2 Letaw's Formula

For such high energies as $T_p > 2$ GeV,

$$\begin{aligned}\sigma(T_p) &= \sigma(\mathrm{h.e.})\\ &= 45A^{0.7}[1+0.016\sin(5.3-2.63\ln A)]\ \ \mathrm{mb}.\end{aligned} \tag{6.4}$$

For 2 GeV $> T_p >$ 10 MeV,

$$\begin{aligned}\sigma(T_p) &= \sigma(\mathrm{h.e.})\\ &\quad\times[1-0.62\exp(-T_p/200)\sin(10.9T_p^{-0.28})].\end{aligned} \tag{6.5}$$

where T_p is in units of MeV.

1) A. Kohama, K. Iida, and K. Oyamatsu, Phys. Rev. C **69**, 064316 (2004).
2) A. Kohama, K. Iida, and K. Oyamatsu, J. Phys. Soc. Japan **85** (2016) [The main body of the whole manuscript] [arXiv:1411.7737].
3) A. Kohama, K. Iida, and K. Oyamatsu, Phys. Rev. C **72**, 024602 (2005).
4) H. de Vries, W. de Jager, and C. de Vries, At. Data Nucl. Data Tables **36**, 495 (1987).
5) E. Friedman and A. Gal, Nucl. Phys. **A724**, 143 (2003).
6) G. F. Bertsch and R. A. Broglia, *Oscillations in Finite Quantum Systems* (Cambridge University Press, Cambridge, 1994).
7) A. Bohr and B. R. Mottelson, Nuclear Structure Vol. I *World Scientific*, (1998).
8) H. Kondo, *Master thesis*, Graduate School of Integrated Arts and Sciences, Kochi University (2013) [in Japanese].
9) R. J. Glauber, *Lectures in Theoretical Physics*, Vol. I, ed. W. E. Brittin and D. G. Dunham (Interscience, New York, 1959), p. 315.

10) K. Iida, A. Kohama, and K. Oyamatsu, J. Phys. Soc. Japan **76**, 044201 (2007).
11) L. Spitzer, Jr., *Physical processes in the interstellar medium* (Wiley Classics Library, 1998).
12) G. Royer, Nucl. Phys. **A807**, 105 (2008).
13) L. R. B. Elton and A. Swift, Nucl. Phys. **A94**, 52 (1967).
14) K. Iida, K. Oyamatsu, B. Abu-Ibrahim, and A. Kohama, Prog. Theor. Phys. **126**, 1091 (2011).
15) H. L. Bradt and B. Peters, Phys. Rev. **77**, 54 (1950).
16) S. Kox, A. Gamp, C. Perrin, J. Arvieux, R. Bertholet, J. F. Bruandet, M. Buenerd, R. Cherkaoui, A. J. Cole, Y. El-Masri, N. Longequeue, J. Menet, F. Merchez, and J. B. Viano, Phys. Rev. C **35**, 1678 (1987).
17) L. W. Townsend and J. W. Wilson, Phys. Rev. C **37**, 892 (1988).
18) W. -Q. Shen, B. Wang, J. Feng, W. -L. Zhan, Y. -T. Zhu, and E. -P. Feng, Nucl. Phys. **A491**, 130 (1989).
19) R. K. Tripathi, F. A. Cucinotta, and J. W. Wilson, NASA Technical Paper 3621 (1997).
20) R. K. Tripathi, F. A. Cucinotta, and J. W. Wilson, NASA Technical Paper TP-1999-209726, (1999).
21) L. Sihver, M. Lantz, and A. Kohama, Phys. Rev. C **89**, 067602 (2014).
22) L. Sihver, C. H. Tsao, R. Silberberg, T. Kanai, and A. F. Barghouty, Phys. Rev. C **47**, 1225 (1993).
23) R. F. Carlson, At. Data Nucl. Data Tables **63**, 93 (1996).
24) The GEM collaboration, H. Machner and B. Razen, Nucl. Instru. Meth. **A437**, 419 (1999).
25) J. R. Letaw, R. Silberberg, and C. H. Tsao, Astrophys. J. Suppl., **51**, 271 (1983).